Characterization of dissolved organic matter in water using Fourier Transform Infrared spectroscopy and X-ray photoelectron spectroscopy: Implication for chemical composition and effects of water sources

---

A Thesis presented to

the Faculty of the Graduate School

at the University of Missouri-Columbia

In Partial Fulfillment

Of the Requirements for the Degree

Master of Science

By

SHICHEN ZHANG

Professor Baolin Deng Thesis supervisor

May 2015

The undersigned, appointed by the dean of the Graduate School, have examined the thesis entitled

CHARACTERIZATION OF DISSOLVED ORGANIC MATTER IN WATER USING FOURIER TRANSFORM INFRARED SPECTROSCOPY AND X-RAY PHOTOELECTRON SPECTROSCOPY: IMPLICATION OF CHEMICAL COMPOSITION AND EFFECTS OF WATER SOURCES

Presented by Shichen Zhang,

A candidate for the degree of Master of Science,

And hereby certify that, in their opinion, it is worthy of acceptance.

Professor Baolin Deng

_____

Professor Matthew Bernards

_____

Professor Paul C. Chan

_____

ACKNOWLEDGEMENT

First and foremost, I would like to express my sincere gratitude to Professor Baolin Deng for his precious advice, encouragement and support all throughout my graduate studies. He inspired me greatly in my research work and motivated me to become a creative and diligent researcher.

Next, I would like to thank Dr. Bin Hua for his willingness to provide me opportunity and guidance in the past two years. He gave me tremendous inspiration and help during my hard time. I would also like to thank Dr. Keith Goyne for his kindness and support. Without his persistent help, the process of my research would be harder and slower.

I would like to thank my committee member, Dr. Matthew Bernards and Dr. Paul Chan, for their help to improve my work and their precious time devoted to my defense and thesis. They offer many constructive suggestions important to complete this project.

Also, I wish to express my appreciation to all the members in Dr. Deng's research group. Jun Yin, Zhe Yang, Zhengyang Wang, Shuang Gao and Zhongyi Shi all provided me assistance and encouragement throughout my school year. I cherished the time working together with all of you.

Last but not the least, an honorable mention goes to my family and friend for their endless love and support, and my partner Mingming for the warmest concern, understand and accompany.

TABLE OF CONTENTS

LIST OF FIGURES

LIST OF TABLES

ABSTRACT

Dissolved organic matters (DOM) from several freshwater sources (Hinkson Creek upstream, Missouri River, landfill leachate, and wastewater treatment plant (WWTP)) were characterized by Fourier transform infrared spectroscopy (FTIR) and X-ray photoelectron spectroscopy (XPS). The goal was to identify major chemical compound classes, such as carboxylic acid, amide, ester, and aliphatic and aromatic characteristics in water samples from different sources. During the FTIR spectra analysis, in addition to the original spectra, their second derivatives were taken in the range of 1000-1900cm^{-1} and analyzed without significant spectral overlapping. For XPS analysis, after survey spectra were obtained, carbon, nitrogen and oxygen high-resolution spectra were collected and analyzed using CasaXPS software, which allowed deconvolution of various peaks for identification of various components. Results showed that samples from the city landfills contained the highest concentration of aromatic and protein-like compounds, while samples from WWTP contained more acids and hydrophilic fraction. It appeared that for freshwaters, the DOM inputs from the surroundings had a significant effect on the DOM chemical composition. The study demonstrated that coupling FTIR with XPS analyses could provide insights into the physicochemical and biogeochemical characteristics of DOM in different aquatic systems, as well as the characteristics of the environments from which the DOMs were derived.

Key words: Dissolved organic matter (DOM), FTIR, XPS, chemical composition, sources

CHAPTER 1

Introduction

Dissolved organic matter (DOM) is the major form of organic matter in most aquatic environments and is one of the largest exchangeable organic reservoirs at the earth's surface. DOM influences the physicochemical characteristics of natural aquatic systems by acting as a carbon and energy source, increasing light attenuation, maintaining pH through organic acid buffering, acting as a strong ligand for many elements, and affecting the heat balance and the redox chemistry of trace metals(Maie, Parish et al. 2006). DOM is chemically heterogeneous and composed of classes of organic substances that can be differentiated based on chemical properties, hydrophobicity or molecular weight (Pérez, Moreira-Turcq et al. 2011).The chemical composition of aquatic DOM, both in terms of functional groups and higher order conformation, can provide significant information about the water quality and the linkage of its source (Minor and Stephens 2008). In recent years, there have been many researches focused on the nature of DOM and its sources and cycling in aquatic systems. Elemental components, such as dissolved organic carbon or nitrogen, and molecular constituents, like amino acids, carbohydrates or lipids, were characterized by various approaches (Yamashita and Tanoue 2003).

Dissolved organic carbon (DOC) may come from bacteria-derived materials, terrestrial watershed and urban sewage (Pernet-coudrier, Clouzot et al. 2008). Dissolved organic

nitrogen (DON), which also plays an important role in freshwater environments, comes mostly from terrestrial runoff, phytoplankton or bacteria release, and its sinks include uptake and degradation by microorganism, photochemical decomposition and abiotic adsorption (Berman and Bronk 2003). Humic substances constitute the largest fraction of DOM in most natural waters and are considered relatively resistant to bacterial degradation (Carlsson, Segatto et al. 1993). The nitrogen-containing fraction of DOM is always comprised of humic substances, which is further classified operationally as humic acids and fulvic acids.

For freshwater systems, DOM transport and modification are greatly affected by interactions between the surrounding landscape and DOM quantity and characteristics. In-stream and water transition zones are also important for organic matter characteristics downstream, and riverine terrigenous (lignin-containing) DOM is more refractory to microbial re-working but highly photodegradable (Stephens and Minor 2010). Landfill, a complex biological system capable of stabilizing solid waste, contains high concentration of DOM and results in the production of leachate with potential hazards to surrounding environment (Bu, Wang et al. 2010, He, Xi et al. 2011). DOM in the raw leachate is a heterogeneous mixture of humic substances, hydrophilic acids and proteins, playing an important role in microbial activity, pollutant degradation and transport of metals (Bu, Wang et al. 2010). In municipal wastewater treatment plants, the effluent after the secondary treatment remains a significant source of DOM. These compounds control the interaction and transport of toxic chemicals and serve as precursor in the chlorination process forming disinfection by-products (Zhang, Qu et al.

2009, Xue, Zhao et al. 2011). As the riverine DOM largely affects aquatic environment and is greatly influenced by surrounding inputs, its chemical composition could provide critical information about the conditions of its source. Many techniques have been applied to detect molecular constituents of water samples, but the linkages with their sources remain unclear. In this study, water samples were collected from both rivers and urban waste areas, in order to investigate the effects from riverine surroundings and human activities, respectively. Fourier transform infrared spectroscopy (FTIR) in conjunction with X-ray photoelectron spectroscopy (XPS) was explored to observe chemical compositions of DOM and differentiate the characteristics of their origins.

FTIR has been widely applied to characterize and differentiate humic substances, composted materials as well as DOM from water samples of different origins and nature. It detects specific functional groups of molecules, resolving the carboxyl, amide and aliphatic ester contributions to DOM(Provenzano, Caricasole et al. 2010). Fundamentally, infrared spectroscopy is based on the vibration of molecules when they are exposed to infrared radiation and each bond in the molecule gets involved in different vibration modes: stretching and bending. Due to the nature of DOM, a mixture of organic compounds could result in an overlap among bands. This makes the more common compounds emerge above the background while the less common bands disappear under the background. One of the resolution enhancement methods is to take the second derivative of the FTIR spectrum, which is widely used in peak identification. XPS is another non-destructive and semi-quantitative technique for estimating the proportions of various species of an element. Photoelectrons ejected from the surface of

a solid sample irradiated by an X-ray beam are analyzed spectrophotometrically with an energy analyzer. XPS can be used to assign the relative abundance of elements in solid samples due to the differences among binding energy of various elements and various electron states of the same element . In this study, XPS technique was applied for investigating the elemental constituent and the concentration of C, N and O species in water samples (Abe and Watanabe 2004). In high-resolution spectra, quantification and peak fitting were processed in the CasaXPS software. A single element signal was deconvoluted into several signals corresponding to different type of compounds and the proportion was estimated respectively.

Eight solid samples isolated from various water sources were analyzed in this study using FTIR and XPS. The characteristics of dissolved organic matter were then deduced in terms of molecular constituents and their linkage to the point and non-point sources were discussed with respect to the sources of water sample. By comparing their molecular compositions, we could better understand the characteristics of riverine DOM originating from different sources. The interaction between DOM and the surroundings was also explored.

CHAPTER 2

Materials and methods

2.1 Sampling sites

In a collaborative project involving the Lincoln University of Missouri, University of Missouri, and Old Dominion University, fourteen sampling sites were selected within Hinkson Creek watershed located in central Missouri, including non-point and point contamination sources as shown in Fig. 1. In the study reported in this thesis, samples from sites 1-2 and 9-14 were used, and all of the serial numbers were unchanged for the convenience of quotes and comparison. The percentages of land use and land cover (LULC) for 1 and 2 catchments are also shown in Fig. 1. Site 1 and 2 were collected from two upstream tributaries of Hinkson Creek primarily in rural areas mixed with cropland and forest, respectively, and considered as non-point source agricultural areas. Site 14 was selected on Missouri River as natural background. Site 9 and 10 were ponded leachates at the city landfill and Site 11 to 13 were within the wastewater treatment plant (WWTP) at the wastewater inlet, constructed wetland inlet, and constructed wetland outlet, respectively. Sites 9-13 were considered as point source areas.

2.2 Sample collection

Water samples were collected monthly from November 2011 to October 2012 at the 14 selected sites, with 168 samples in total. Common water quality parameters, including pH, dissolved oxygen and electrical conductivity, were measured onsite when samples

were collected. The collected water samples were transported to laboratory in coolers and stored at 4°C in a refrigerator prior to analysis. All water samples were filtered

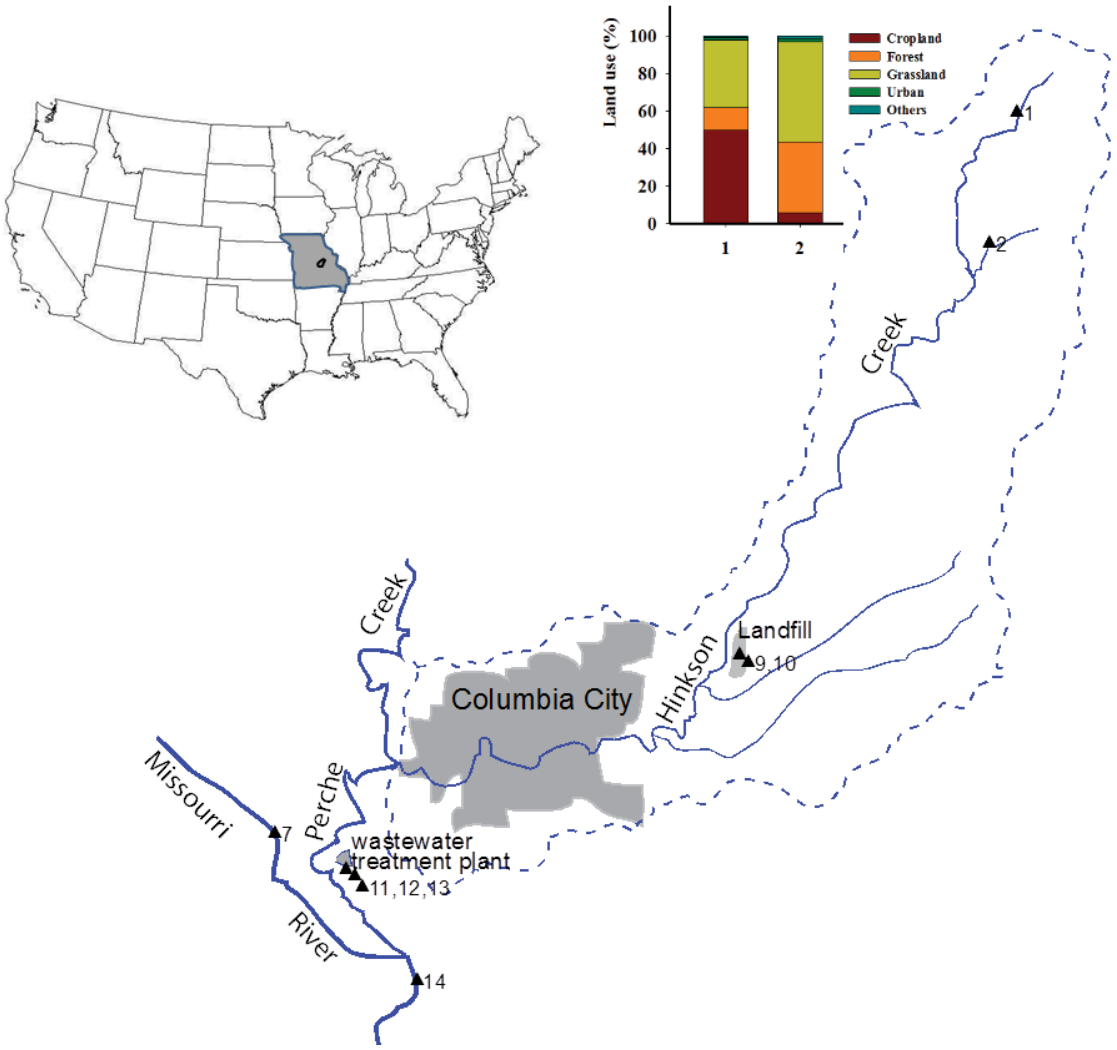

Figure 1 Map of the study area in the United States, sampling sites and land use with site 1 and 2. The dashed line encloses the watershed of the Hinkson Creek. Solid triangles indicate the locations of water sampling sites and the numbers behind represent the codes of the water samples.

through 0.45 μm syringe filters (Fisher Scientific) before analysis. Eight solid DOM samples were isolated from selected water samples to better analyze the DOM structure. Fort the DOM isolation, 200 L water samples were collected from Site 1 and 2 (non-point source), and 14 (background), and 5-10 L samples from Site 9 to 13 (point sources), followed by filtration through 1.2 μm and then 0.45 μm membrane filters (Whatman Co.). Samples from site 1, 2, and 14 were further concentrated through a reverse osmosis process with Realsoft to ~20 L. The reverse osmosis pretreatment was not applied to the samples from site 9 to 13 as they were relatively concentrated to begin with. Afterwards, a two-stage evaporation was applied, with the first stage at 80-85°C and the second stage at 50°C to minimize the impact of high temperature on DOM chemical properties. In this way, the water samples were evaporated at 80-85°C in a rotary evaporator (LabConco Co.) to <100 mL volume, followed by oven- drying at 50°C. The solids were stored in a refrigerator until further analysis.

2.3 FTIR analysis

The solid samples were analyzed by FTIR using a Nicolet 4700 FTIR spectrometer (Thermo Electron Corp, Madison, WI) equipped with a diffuse reflectance infrared Fourier transform (DRIFT) Smart Collector accessory (Thermo Electron Corp.), blank corrected with KBr background spectra. Samples were prepared by mixing the material with KBr at the mass ratio of 1:9. Then the mixtures were ground gently with a mortar and pestle. For background (or baseline) correction, a KBr pellet without sample was analyzed prior to other samples. After inserting the mixture into the spectrometer, the intake pipe was opened first in order to let nitrogen fill the instrument. This

preparation took 15 minutes every time before analyzing each mixture, then the analysis would take another 400 seconds to complete the process.

FTIR results were analyzed in terms of both absorption spectra and their secondary derivative spectra. Original absorption spectra were recorded directly from the spectrometer, and the secondary derivative spectra were calculated by Resolutions Pro software in the range from 1000 cm^{-1} to 1900 cm^{-1} in order to deconvolute the overlap in this range. The secondary derivative spectra are interpreted in discussion section as additional evidence.

2.4 XPS analysis

The solid DOM samples were analyzed using a Kratos Axis 165 Photoelectron Spectroscopy System. The samples were placed on a conductive carbon tape in conductive sample holders and analyzed in the chamber under a 10^{-8} Torr ultrahigh vacuum. To obtain the best elemental resolution, the monochromatic Al source was used for excitation with pass energy at 80 eV. A charge neutralizer was also used to further reduce the effects of differential or sample charging. A broad range survey was collected for each sample before Ar gas sputtering of the solid surface. After gentle sputtering of the surface, high resolution scans for N, O, and C were recorded for each sample.

The data manipulation, including deconvolution, integration and intensities calculation, was accomplished on CasaXPS software (Sansotera, Persico et al. 2013). A linear

background was selected as the base line in each spectrum. Then a standard line shape analysis with a Lorentzian-Gaussian fitting function was used(Chan, Gallard et al. 2012). The proportions of different functional groups for each specific element were estimated from the relative areas surrounded by Gaussian curves and the base line with respect to the spectral area(Abe, Maie et al. 2005).

CHAPTER 3

FTIR results

The general assignments of FTIR spectra are shown in Table. 1. The assignments were classified by different functional groups then categorized into several compound classes. Table. 2 showed peak intensity of the FTIR spectra of all solid samples. Each peak in the spectra was described as a strong, medium or weak band in the table. According to the principle in Table.1, peaks in FTIR spectra of eight solid samples were identified and presented in terms of the band assignments in Table. 3. The characteristic of each assignment and their compound classes were also listed. In addition, the results from the secondary derivative FTIR spectra are presented in the discussion part, including the peak position and assignment of each compound class.

Table 1 General assignments of FTIR spectra of DOM fractions (Minor and Stephens 2008, Xue, Wang et al. 2009, Bu, Wang et al. 2010)

Absorption (cm^{-1})	Assignment	Compound class
3300-3400	O-H	Carboxylic groups
3200	N-H	Amide, amidocyanogen
2800-3000	CH_2, CH_3	Alkyl, aliphatic C-H, alkane
2500	O-H	Carboxylic groups
1735-1700	C=O	Carboxylic and carbonyl groups
1690-1650	C=O	Amide-1
1620-1580	C=C, COO-	Aromatic groups, ester
1570-1540	N-H, C-N	Amide-2
1520-1500	C=C, C=N	Lignin, aromatic groups
1480-1380	CH_2, CH_3, C=O-H	Aliphatic groups
1240-1150	C-O, C-O-C	Carboxylic acid, alcohol, ester, ether
1120-1000	C-O, O-H	Carbohydrate, ester, polysaccharide or polysaccharide-like substances
850-650	C-H	Alkyne, aromatic

Table 2 Peak intensities in FTIR spectra for eight solid samples: sample 1, 2 and 14 from freshwater sources; sample 9 and 10 from city landfill; sample 11, 12, 13 from wastewater treatment plant (WWTP).

Assignment And Position (cm^{-1})	Carbohydrate 1030-1130	Aliphatic 1390-1460	Aromatic 1570-1590	Amide 1630-1670	Carbonyl 1780-1830	Hydroxyl 3290-3400
Sample 1, 2	Medium in site 1, strong in site 2	Both strong	Medium in site 1, none in site 2	None	Small, weak	Medium and broad
Sample 9, 10	Both medium	Both strong	Both medium, as shoulder	Small, side peak	Small, weak	Medium and broad
Sample 11, 12, 13	All strong, multiple band contained	Medium in site 11 and 12, sharp in 13	None	Medium in site 11, sharp in 12 and 13	Small in site 11, sharp in 12 and 13	Strong and Broad
Sample 14	Strong	Medium	Medium	Sharp	Small	Strong and broad

Table 3 Peak assignment in FTIR spectra of each solid samples: sample 1, 2 and 14 from freshwater sources; sample 9 and 10 from city landfill; sample 11, 12, 13 from wastewater treatment plant (WWTP).

Wavenumber (cm^{-1})				Assignment	Compound class	Remark
Sample 9-10	Sample 11-13	Sample 1-2	Sample 14			
3320-3350	3300-3390	3290-3360	3370	O-H	Carboxylic acid, alcohol	Stretching of hydroxyl groups from hydrogen bonding
2930-2960	2850-2930	2950-2970	None	C-H	Alkyl, aliphatic group, alkane	Asymmetrical and symmetrical stretching of methyl and methylene; protein signal in humic substances and organic matter in water
2500-2520	2500-2520	2510	2520	O-H	Carboxylic acid	Weak broad band for carboxylic stretch
Around 1670	1630-1650	None	1650	C=O, C=C	Amide	Stretch of amide I groups or aromatic esters
1570-1580	None	1590	1540	C=O, N-H	Aromatic group, amide	Aromatic double bonds that are conjugated with COO-, and N-H bending of amide-2 groups
1440-1460	1400-1440	1390-1440	1420	CH_2, CH_3, C-O-H	Aliphatic group	Aliphatic C-H deformation, carboxylic acid in-plane C-O-H bending
1050-1120	1050-1170	1020-1030	1130	C-O, C-O-C, O-H	Carbohydrate, ester, phenol, alcohol	Signal of polysaccharide or polysaccharide-like
877-881	870-872	835-876	854	C-H, N-H	Alkyne, aromatic group	C-H vibration or aromatic signal, N-H bending
Around 619	609-615	617-619	615	C-Cl	Chlorocompound	Vibration of halogenated functions like C-Cl stretch of aliphatic chlorocompound

3.1 FTIR spectra for DOM in landfill leachates and its chemical composition

FTIR spectra of the solid samples collected from the ponded leachates of two different landfill cells are very similar, as shown in Fig. 2. Each spectrum has a broad absorption peak in the high frequencies with a maximum absorbance at around 3320-3350cm^{-1}, which results from O-H stretching of organic functional groups in alcohols or acids. Because both of them are very close to 3300cm^{-1}, they may also be assigned to stretching vibration of C-H in alkyne. In both spectra, an additional smaller absorption on the left side of the broad peak shows evidence of aliphatic C-H stretching bands, observed at 2960 and 2930cm^{-1}, respectively. The C=C stretching of aromatic vibration or the C=O asymmetric stretching of deprotonated carboxylic acid(Abdulla, Minor et al. 2010) at 1580cm^{-1} suggested the presence of humic substances or recalcitrant organic materials(Stephens and Minor 2010) in both samples. On the other hand, the peaks around 1670cm^{-1} are also likely related to C=O of amide groups, while the peaks around 1580cm^{-1} might be N-H bending bands of primary or secondary amide, which indicates the presence of nitrogen compounds, likely from protein(Pérez, Moreira-Turcq et al. 2011). Both sources featured intense and relatively sharp peaks at about 1440-1460cm^{-1}, likely due to C-H bending bond in alkane. Two spectra showed strong and broad peaks of lower intensity with maximum absorbance at around 1050-1120cm^{-1}, which generally assigned to C-O stretching from alcohols, phenols or ethers. Beside that, these peaks also suggest probable existence of oxide, such as S=O in sulfoxide, P=O in phosphate or Si-O in silicates. Within the frequencies interval from 600cm^{-1} to 900cm^{-1}, there are very strong and sharp bands at 881cm^{-1} and 877 cm^{-1} respectively in each spectrum, usually resulting from C=CH bending in alkene, N-H bending in amine or esters consisted by P and S. Finally, peaks at

696cm^{-1} and 619cm^{-1} were assigned to the vibration of halogenated functional groups like C-Cl stretching of aliphatic chlorocompounds(Xue, Wang et al. 2009).

By comparing these two spectra, I found some differences at lower intensity of frequencies. The most noticeable difference is at around 1050-1120cm^{-1}. There is only one strong and broad band at 1100cm^{-1} for sample 9, while there are two relatively broad bands at 1050cm^{-1} and 1120cm^{-1} for sample 10. Those two bands may be attributed to C-O stretching vibration in carboxylic acid or ester groups. Additionally, the peak at about 619cm^{-1} for sample 9 is much stronger than that for sample 10, which showed more significant amounts of halogenated compounds contained in sample site 9.

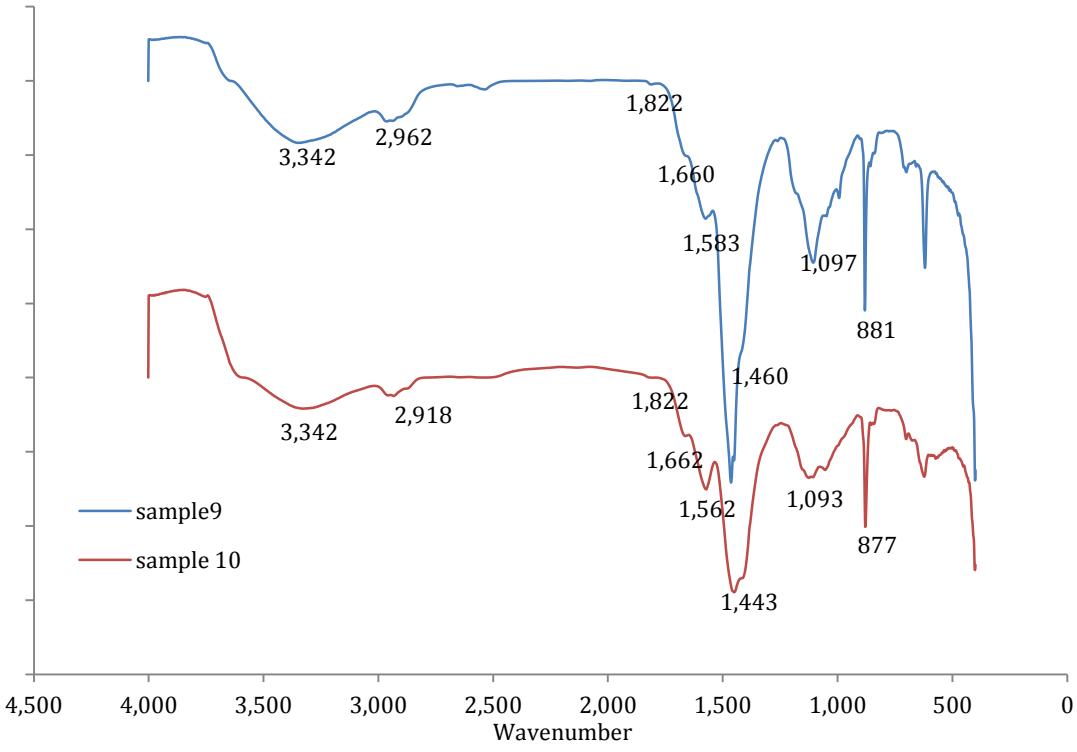

Figure 2 FTIR spectra of solid samples from different sites: sample 9 and 10 were both from city landfill leachates.

3.2 FTIR spectra for DOM in wastewater treatment plant and its chemical composition

FTIR spectra of the solid samples collected from the inlet and outlet effluents of the wastewater treatment plant are found in Fig. 3. There are many similarities among these samples. In the higher frequencies, the broad humps in the range from 3000cm^{-1} to 3600cm^{-1} in each spectrum are due to the stretch of O-H bonds in alcohols, the O-H stretch in carboxylic acids and/or the N-H in amides. Small and mild waves appear in the region from 2850cm^{-1} to 2950cm^{-1} with maximum absorption at 2930cm^{-1}, 2850cm^{-1} and 2760cm^{-1}, respectively, in three spectra. They are assigned to aliphatic C-H, C-H_2 and C-H_3 stretching (Xue, Wang et al. 2009). The bands in the 1630-1650cm^{-1} region are assigned to C=O stretching of amide groups or the aromatic C=C vibration. There are tiny but sharp peaks at around 1790cm^{-1} attributed to C=O stretch in carboxylic acid. A relatively strong peak is observed at 1400cm^{-1} or 1440cm^{-1} of each spectrum, likely due to aliphatic C-H deformation in alkane, asymmetric stretching in carboxylate or C-O-H stretching of phenolic or carboxyl groups (Stephens and Minor 2010, He, Xi et al. 2011). One of the most prominent wavebands in each of the spectra is a strong peak at around 1050-1170cm^{-1}, resulting from the C-O stretch of polysaccharides, long chain fatty acids or ethers (Stephens and Minor 2010). When comes to the lower frequencies, all three spectra were characterized by sharp bands at around 835-872cm^{-1} for substituted aromatics and C=C bending in alkenes (Landry and Tremblay 2012). Additionally, the 610-615cm^{-1} bands are associated to C-Cl stretching in alkyl halides.

Differences occur on relatively lower frequencies among the three spectra. There is only a single peak at 1130cm^{-1} for sample 11, while peaks at the same position divided into three or four small peaks ranging from 1050 to 1170cm^{-1} in other spectra. This may be caused by C-O stretching which contains multiple bands in esters or acids. Additionally, in the region of 1800cm^{-1}, only weak and mild waves appeared from the sample 11 while sharper and stronger peaks appear in sample 12 and 13, indicating an increased concentration of carboxylic acids along the wastewater treatment plant.

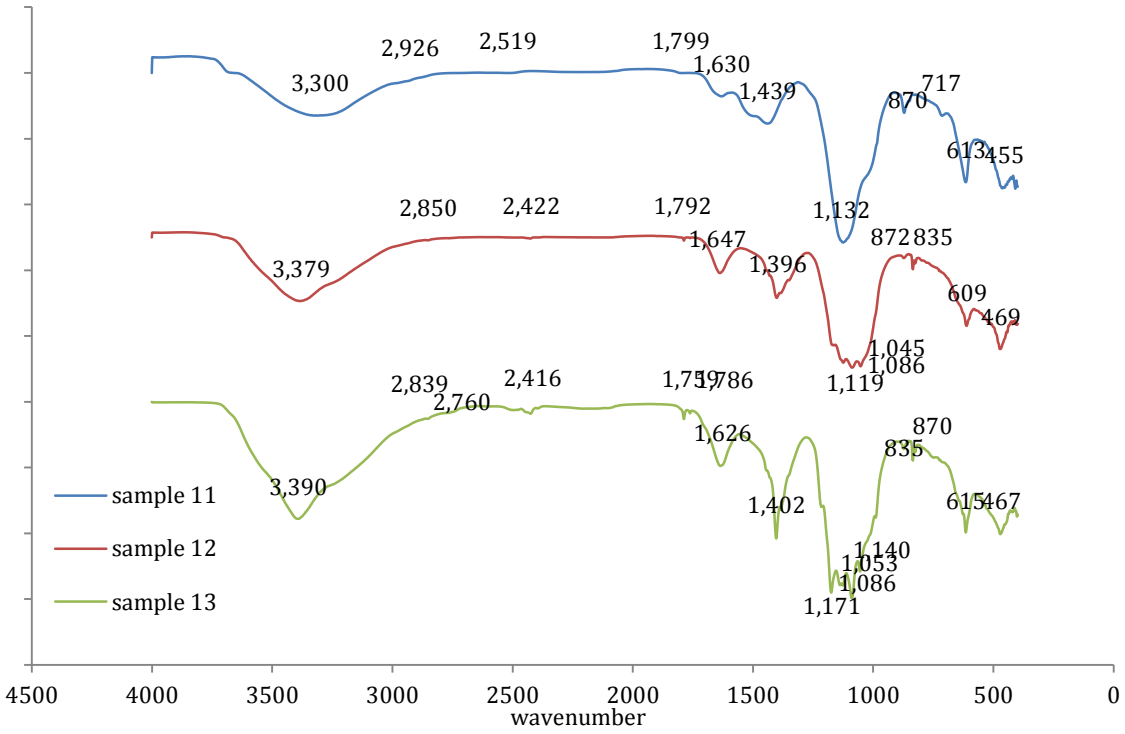

Figure 3 FTIR spectra of solid samples from different sites: sample 11, 12, 13 were from wastewater treatment plant (WWTP) on the inlet of wastewater, inlet of constructed wetland, outlet of constructed wetland, respectively.

3.3 FTIR spectra for DOM in upstream of Hinkson Creek and its chemical composition

FTIR spectra of the solid samples from upstream of Hinkson Creek surrounded by cropland and forest are found in Fig. 4. These two spectra are very similar to each other in the position and shape of the principal absorption bands at higher frequencies. In the region below 1800cm^{-1} wavenumber, they vary from each other in terms of the position and intensity of the main absorption peaks. In the region above 1800cm^{-1} wavenumber, both spectra were characterized by strong broad bands at about 3360cm^{-1} for H-bonded OH groups of alcohols, phenols and organic acids, as well as H-bonded N-H groups of amines and amides (Abdulla, Minor et al. 2010). Spectra also show evidence of aliphatic C-H stretch in alkanes around 2930-2950cm^{-1}. A weak but broad bump was observed at 2430cm^{-1} and 2510cm^{-1} of each spectrum, respectively. There likely indicate the presence of sulfur and phosphorus compounds. In the region around 1800cm^{-1}, both spectra have small bands which were assigned to the vibration of C=O carboxyl groups (Chen, Zhou et al. 2010).

In the region below 1800cm^{-1} of the spectrum of the sample 1, a relatively mild broad peak at 1590cm^{-1} is attributed to C=C stretching of aromatics, C=O stretching of acids or amides. The aliphatic C-H bending bands were observed strongly and sharply at medium frequencies (1390cm^{-1}) (Chen, Zhou et al. 2010). A absorption at 1030cm^{-1} is generally assigned to C-O asymmetric stretching of carbohydrates, such as polysaccharides or aromatic ethers and Si-O bond stretching of silicates (Provenzano, Caricasole et al. 2010, He, Xi et al. 2011). Multiple bands are found at 800-900cm^{-1} indicated that C=C bending

bands in aliphatic alkenes or aromatics are present. At low frequencies, peaks at around 617cm^{-1} were assigned to C-Cl stretching in alkyl halides.

Compared with sample 1, sample 2 from forest-dominated land has much more intense peaks at 1020cm^{-1} and 1440cm^{-1}. Beside that, there is only a single peak at around 850cm^{-1} instead of multiple peaks.

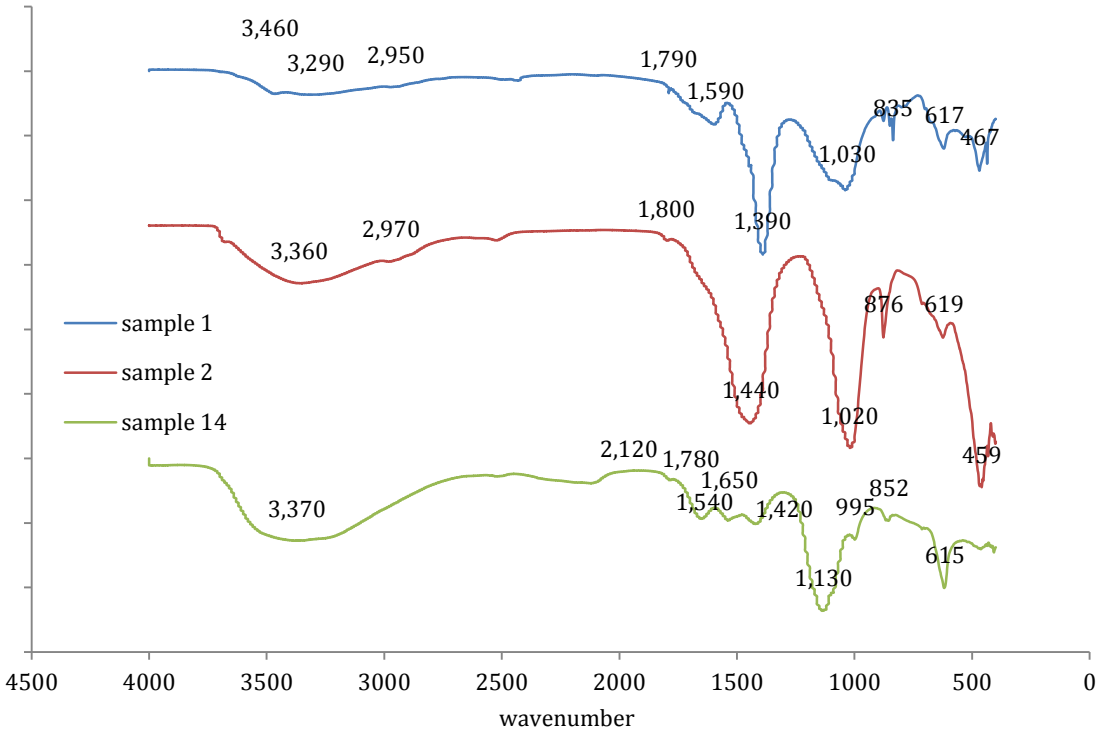

Figure 4 FTIR spectra of solid samples from different sites: sample 1 and 2 were from upstream of Hinkson creek, sample14 was from Missouri river.

3.4 FTIR spectrum for DOM in Missouri River and its chemical composition

The FTIR spectra of the solid samples collected from Missouri River as a natural background is presented in Fig. 4. Compared to all the spectra above, a much broader band in the range from 2800-3650cm-1 was observed as the O-H stretch. A sharp peak at 1130cm^{-1} and medium broad peaks at 1400-1600cm^{-1} indicates much similarity between Missouri river sample and the samples from wastewater treatment plants. Continuous medium peaks appear in region of 1400-1600cm^{-1},which are likely assigned to C=C multiple stretch bonds in aromatics and C=O and N-H stretch bonds in amides. At lower frequencies, the bands are similar to the bands of sample 11-13 described above. However, there is a mild broad band that emerged at 2120cm^{-1} characterized as C=C and C=N stretching vibration of C=C=C, N=C=N or other similar groups, or C≡C stretch in alkynes(He, Xi et al. 2011).

3.5 Summary

Comparing FTIR spectra of the samples from similar sources, we found their spectra have similar basic shape with each other. For example, sample 9 and 10 were both from city landfill cells and, as shown in Table 2 and Table 3, their peak intensity and position was almost the same. Parallel features were found in sample 11, 12 and 13, which all came from wastewater treatment plant. As for samples from freshwater systems, sample 1 and 2 were similar but still contained differences, such as the disappearance of the peak at around 1590 cm^{-1} in sample 2. Sample 14 that came from Missouri river had some similarities to the WWTP samples in basic shape, but the intensity of same specific bands was apparently various.

When it comes to the comparison among samples from different sources, differences appeared in both peak position and intensity. From Table.2, the strongest bands in sample 9 and 10 were C-H bands at around 1400cm^{-1}, while the most intense peaks in sample 11-13 were C-O bands of carbohydrates, which appear around 1030 cm^{-1}. No peak was seen around 1650 cm^{-1} in sample 1 and 2 but such a peak appeared in all of the rest of the samples.

There seems to be a variation trend regarding the chemical composition among these samples. An increase of C-O containing components, like carbohydrates and ethers, took place in the solid samples from sample 1 to sample 14. In addition, an enhancement of aromatic and amide bands (at around 1650 cm-1) and a slight weakening of aliphatic group concentrations appeared along the same observed routine. No obvious trend for N-H containing secondary amide (peak at 1580 cm-1) and carbonyl bands (1790 cm-1) was found. This might result from the impact of overlapping peaks, which enhance the need for FTIR secondary derivative spectra.

XPS results

In the study, all of the samples collected from point and non-point sources were analyzed by XPS to investigate the elemental composition and chemical states. The survey spectra reveal the presence of three major elements: nitrogen, carbon and oxygen. A few of them show the presence of silicon as another important element as well. Atomic compositions for each sample were calculated using wide-scan region areas and the appropriate sensitivity factors of each element (Song, He et al. 2012).

3.6 Atomic concentration of water samples

The atomic concentration of eight samples are shown in Table. 5. Carbon and oxygen clearly dominated the chemical composition. The weight percentage of carbon measured by XPS was in the range from 28% to 44%, while the weight percentage of oxygen was also in the range from 26% to 44%. The elemental ratio among the main elements is presented in Table 6. Concentration of carbon was selected as the denominator when calculating all ratios. The most desired ratios in this study were O/C, N/C and Cl/C, which were further used for characterization of chemical constituents, hydrophobic properties and chlorination effects in water samples.

Table 4 Atomic concentration of main elements and relative parameters in XPS wide-scan spectra from each solid sample: sample 1, 2 and 14 from freshwater sources; sample 9 and 10 from city landfill; sample 11, 12, 13 from wastewater treatment plant (WWTP)

Sample ID	Name	Position	FWHM	Area / (T*MFP)	Atomic Concentration	Mass Concentration
1	O 1s	529	2.731	8378	36.48	30.66
	N 1s	402	1.931	220.36	1.56	1.15
	C 1s	282.5	2.224	2003.43	25.56	16.13
	Na 1s	1069	2.054	13070.43	19.57	23.64
	Sc 2s	500	1.953	593.70	2.60	6.15
	Cl 2p	197	2.592	603.72	3.36	6.27
	Si 2p	100.5	2.556	694.95	10.85	16.01
2	O 1s	529.5	2.312	6914.3	30.14	27.41
	C 1s	283	2.489	3607.14	46.08	31.46
	N 1s	396.5	1.967	390.15	2.77	2.20
	Na 1s	1069.5	2.113	6118.23	9.17	11.99
	K 2s	376	3.459	491.42	2.77	6.15
	Kr 3d	288	1.194	161.13	1.26	5.98
	Cl 2p	197	3.192	996.84	5.56	11.21
	Si 2p	100	2.539	144.27	2.26	3.60
9	O 1s	529.5	2.364	3578.71	26.57	21.18
	C 1s	282.5	2.587	1400.58	30.47	18.23
	N 1s	396	2.554	122.46	1.48	1.03
	Na 1s	1069.5	2.168	9486.78	24.22	27.75
	K 2s	375.5	2.983	241.07	2.31	4.5
	Kr 3d	215.5	3.612	241.6	0.95	3.96
	Cl 2s	268	2.378	790.3	10.17	17.97
	Si 2p	100	2.284	144.13	3.84	5.37
11	O 1s	530	2.25	7031.91	36.05	30.8
	C 1s	283	2.723	2294.78	34.47	22.11
	N 1s	397.5	2.758	289.24	2.41	1.81
	Na 1s	1070	2.203	4416.95	7.79	9.56
	K 2s	375.5	2.652	141.69	0.94	1.96
	Cl 2p	197	3.327	1120.74	7.35	13.92
	S 2p	167	2.286	592.49	5.3	9.07
	Si 2p	100.5	1.994	122.11	2.24	3.37
	Ca 2p	350	3.063	1167.3	3.46	7.4
12	O 1s	530	2.577	7408.63	33.03	24.69
	C 1s	283	2.97	2150.42	28.09	15.76
	N 1s	405	1.969	546	3.96	2.59
	Na 1s	1070	2.661	5916.9	9.07	9.74
	Ca 2p	350	3.073	1324.74	3.41	6.39

	K 2p	291.5	1.927	417.13	1.37	2.51
	Sr 3p	268	3.212	1093.94	2.16	8.84
	Cl 2p	197.5	3.398	1949	11.12	18.42
	S 2p	167.5	2.795	597.31	4.64	6.96
	Si 2p	100.5	2.236	195.74	3.13	4.11
13	O 1s	530	2.516	6507.58	30.11	22.26
	C 1s	283.5	3.437	2322.66	31.49	17.48
	N 1s	397.5	2.316	371.5	2.8	1.81
	Na 1s	1070	2.45	4181.08	6.65	7.07
	Sc 2s	500.5	1.979	221.37	1.03	2.14
	Ca 2p	350.5	3.556	1796.16	4.8	8.9
	Sr 3p	268.5	2.864	912.37	1.87	7.57
	Cl 2p	197.5	3.241	2363.44	13.99	22.93
	S 2s	231.5	3.454	240.62	2.28	3.38
	Si 2p	101	2.354	300.16	4.98	6.46
14	O 1s	530	2.114	11983.59	46.18	38.93
	C 1s	283	2.237	2279.92	25.74	16.29
	Na 1s	1069.5	1.852	6663.43	8.83	10.70
	Ca 2p	350	3.266	1765.87	3.93	8.30
	Cl 2p	197.5	3.132	643.54	3.17	5.93
	S 2p	167.5	2.33	1344.9	9.04	15.27
	Si 2p	101	2.473	224.43	3.10	4.59

Table 5 Elmental ratio in XPS wide-scan spectra from each solid sample, selected the concentraion of carbon as the denominator: sample 1, 2 and 14 from freshwater sources; sample 9 and 10 from city landfill; sample 11, 12, 13 from wastewater treatment plant (WWTP).

Ratio (/C1s)	1	2	9	11	12	13	14
C 1s	1.0000	1.0000	1.0000	1.0000	1.0000	1.0000	1.0000
Cl 2p	0.1316	0.1207	0.3339	0.2133	0.3958	0.4443	0.1233
N 1s	0.0611	0.0601	0.0486	0.0700	0.1411	0.0889	
Na 1s	0.7657	0.1991	0.7950	0.2259	0.3229	0.2113	0.3430
K 2s		0.0600	0.0758	0.0272	0.0489		
Kr 3d		0.0272	0.0311				
O 1s	1.3753	0.6542	0.8721	1.0458	1.1758	0.9562	1.7939
Sc 2p	0.1020					0.0328	
Si 2p	0.4246	0.0490	0.1260	0.0651	0.1114	0.1582	0.1205
Ca 2p				0.1003	0.1215	0.1525	0.1528
S 2p				0.1537	0.1653	0.0724	0.3511
Sr 3d					0.0768	0.0593	

3.7 Carbon functional groups

C1s XPS is a powerful tool to determine the nature of the various types of carbon. It provided information on the speciation of nitrogen-linked carbon and oxidized carbon in different states (Templier, Miserque et al. 2012). In our study, all the C1s and O1s components obtained by curve fitting were calibrated and referenced to 284.6 eV for C_xH_y type of carbon (Zhao, Wang et al. 2008). Thus, the C1s spectrum enables the distinction among amide, ester and other oxygenated carbon, and the relative peak areas were calculated for the evaluation of atomic concentration. According to previous literatures, four types of C bonds were initially considered to deconvolute the spectra: C bound only to C and H which is assigned to aliphatic and aromatic carbon (C-C, C=C and C-H), C singly bound to O or N, including ether, alcohol and amine (C-O, C-N), C bound to O using two single bonds, including amide, carbonyl, carboxylate, ester (C(O)O, C(O)N), C bound to O using a double bond, including acetal and hemiacetal (O-C-O) (Liao, Lin et al. 2011). Table. 6 showed the principle of XPS peak assignment with respect of peak position. According to the table, these carbon bonds were divided by different oxidation states with their positions shown as follow: The underivatized carbon (C-(C, H), C=C) is at a binding energy of 284.6-285.5 eV, the mono-oxygenated carbon (C-O, C-N), is at a binding energy of 285.6-287.45 eV, and the di-oxygenated carbon (C=O, O-C-O) is at a binding energy of 287.4-288.0 eV. In the higher energy interval, carboxyl carbon (O-C=O) is at 288.5-290.0 eV and amide carbon (N-C=O) is at 287.5-288.7 eV (Eriksson, Frankki et al. 2004).

The high-resolution C1s spectra of eight samples are found in Fig. 5., with the binding energies, assignments and quantitative data for each peak in Table. 7.

Table 6 Principle of XPS peak assignment for carbon, nitrogen and oxygen high-resolution spectra with respect to peak position

Type of carbon	Expression	Binding energy (eV)
Underivatized	C-(C,H); C=C	284.6-285.5
Mono-oxygenated	C-O; C-N; C-Cl	285.6-287.5
Di-oxygenated	C=O; O-C-O	287.4-288.0
Carboxyl and amide	O-C=O; N-C=O	287.5-288.7
Type of nitrogen	Expression	Binding energy (eV)
Mixture	CH3CN; NH3	397.2-398.8
Aromatic	Imine, Aromatic amine	Around 399.0
Peptide	Pyrrole, amide-2, tertiary amine, imine	Around 400.4
Primary	Protonated amine	Around 402.3
Inorganic	KNO2; NaNO3	403.3-408.0
Type of oxygen	Expression	Binding energy (eV)
Oxygen oxide	AxOy	529.4-529.7
Carbonyl oxygen	C=O	531.4-531.5
Hydroxide	C-O	532.1-532.9
ester	O-C=O	533.2-534.0

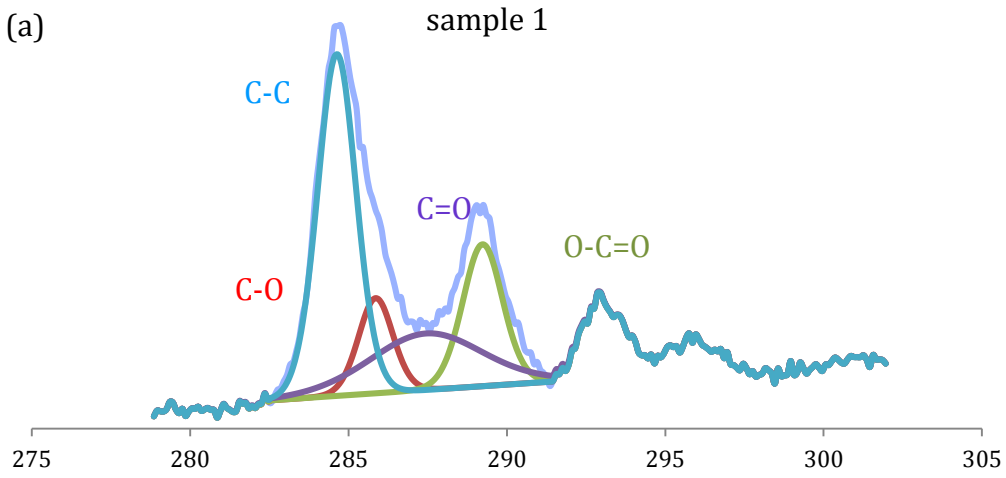
(a)
sample 1
C-C
C=O
O-C=O
C-O
275
280
285
290
295
300
305

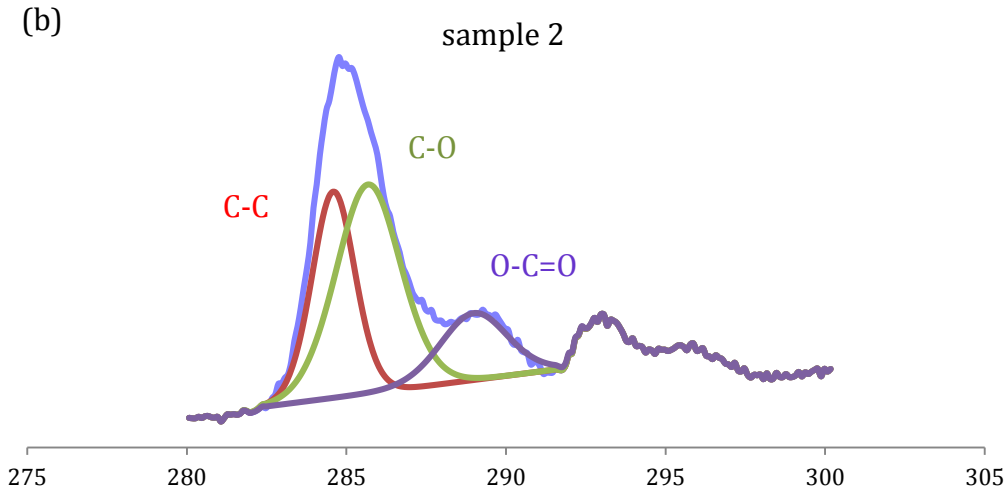
(b)
sample 2
C-O
C-C
O-C=O
275
280
285
290
295
300
305

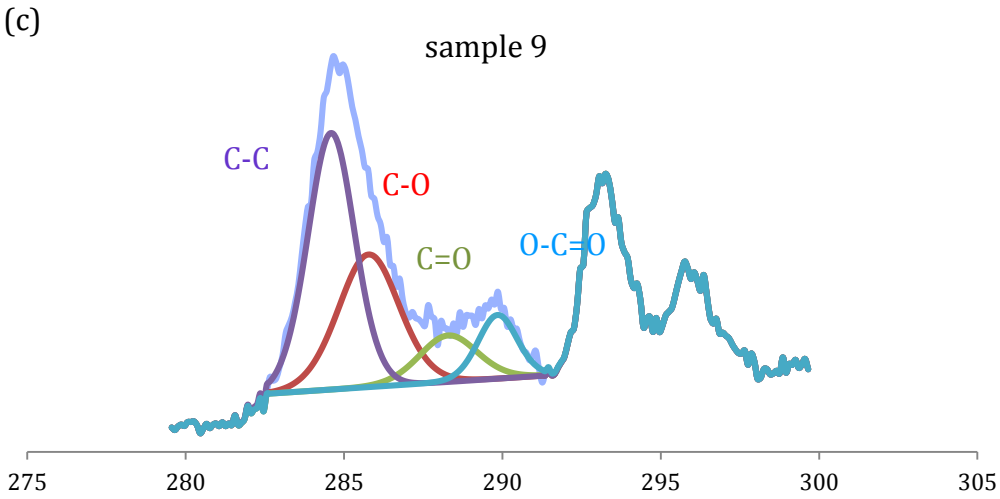
(c)
sample 9
C-C
C-O
C=O
O-C=O
275
280
285
290
295
300
305

(d)

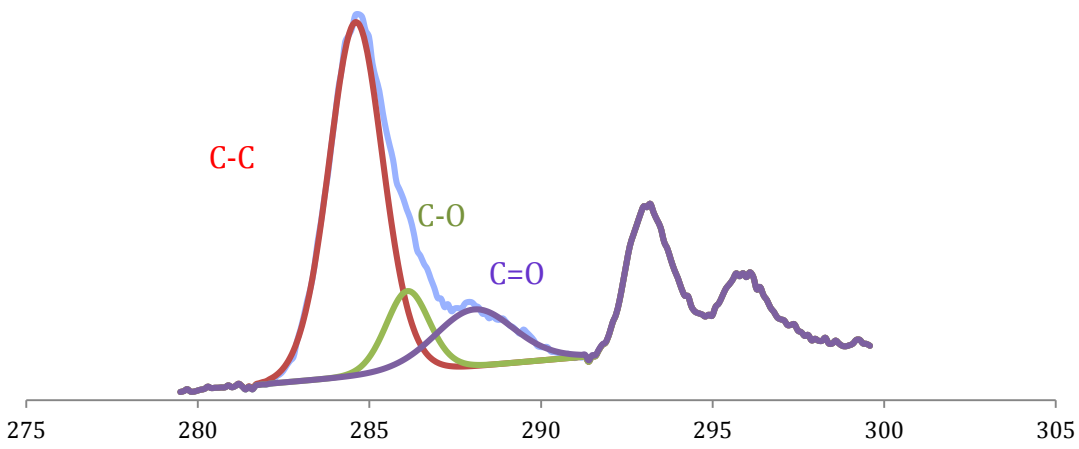
sample 10
C-C
C-O
C=O
275
280
285
290
295
300
305

(e)

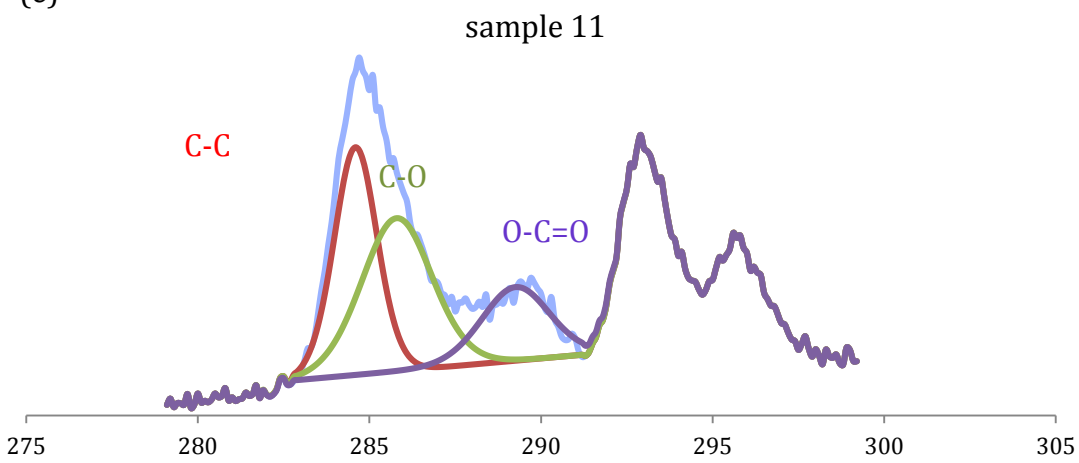
sample 11
C-C
C-O
O-C=O
275
280
285
290
295
300
305

(f)

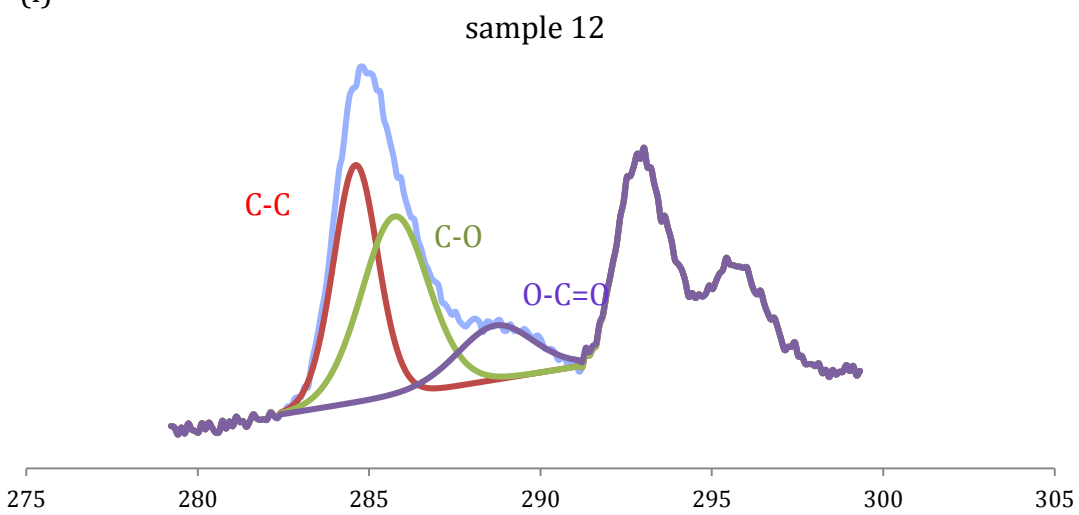
sample 12
C-C
C-O
O-C=O
275
280
285
290
295
300
305

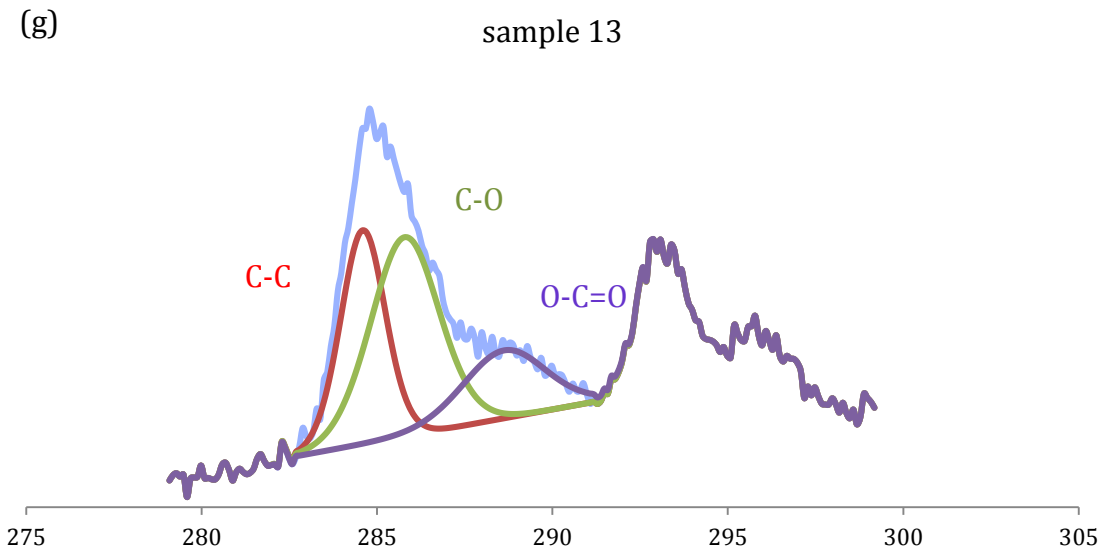

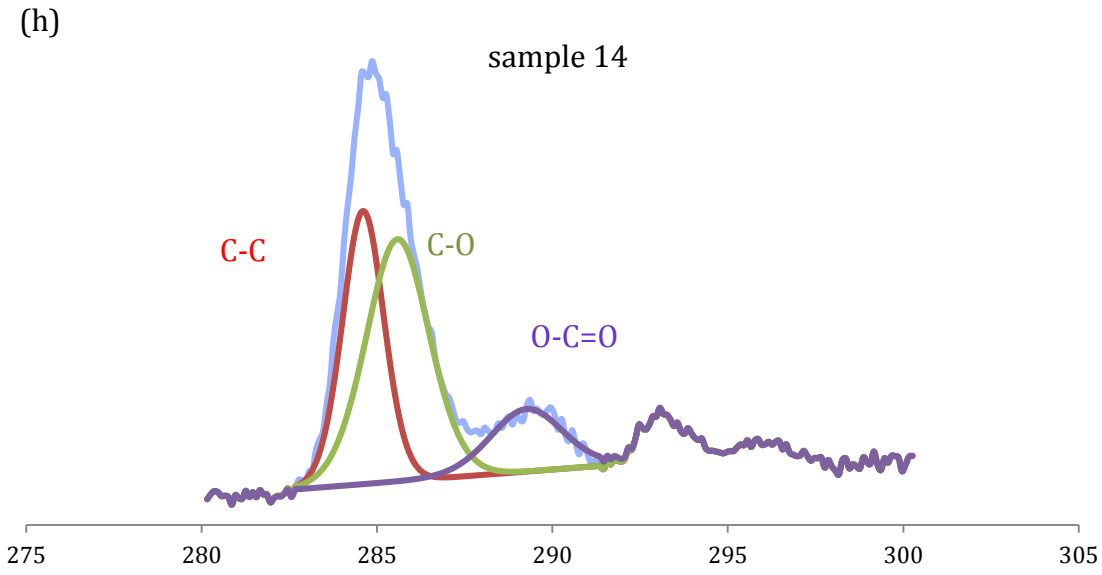

Figure 5 XPS high-resolution C1s spectra of solid samples from different sites: sample 1 (a) and 2 (b) from upstream of Hinkson creek; sample 9 (c) and 10 (d) from city landfill; sample 11 (e), 12(f) and 13 (g) from WWTP; sample 14 (h) from Missouri river. In each sample, light lines are original spectral lines; dark lines are lines of synthesis components.

Table 7 Position, concentration and assignment of synthesis components in XPS C1s high-resolution spectra from each solid sample: sample 1, 2 and 14 from freshwater sources; sample 9 and 10 from city landfill; sample 11, 12, 13 from wastewater treatment plant (WWTP).

Sample ID	Block Id	Position	FWHM	Area/(RSF*T*MFP)	Atomic Concentration	Assignment
1	C 1s/1	284.63	1.431	1178.53	46.33	C-C, C=C
	C 1s/2	285.86	1.283	293.435	11.54	C-O
	C 1s/3	287.46	4.177	566.344	22.26	C=O
	C 1s/4	289.24	1.483	505.445	19.87	O-C=O
2	C 1s/1	284.59	1.582	1538.33	33.01	C-C, C=C
	C 1s/2	285.68	2.383	2344.43	50.31	C-O
	C 1s/3	288.99	2.466	777.133	16.68	O-C-O
9	C 1s/1	284.6	1.747	936.256	47.69	C-C, C=C
	C 1s/2	285.78	2.262	625.475	31.86	C-O
	C 1s/3	288.29	2.155	208.372	10.61	C=O
	C 1s/4	289.85	1.457	193.116	9.84	O-C=O
10	C 1s/1	284.6	1.858	3102.12	70.63	C-C, C=C
	C 1s/2	286.12	1.485	564.995	12.86	C-O
	C 1s/3	288.06	2.714	724.74	16.5	C=O
11	C 1s/1	284.6	1.476	611.864	38.29	C-C, C=C
	C 1s/2	285.79	2.416	673.327	42.14	C-O
	C 1s/3	289.26	2.332	312.671	19.57	O-C=O
12	C 1s/1	284.6	1.531	679.088	39.61	C-C, C=C
	C 1s/2	285.74	2.292	769.32	44.88	C-O
	C 1s/3	288.68	2.628	265.841	15.51	O-C=O
13	C 1s/1	284.6	1.501	511.235	33.2	C-C, C=C
	C 1s/2	285.79	2.299	728.885	47.33	C-O
	C 1s/3	288.62	2.779	299.904	19.47	O-C=O
14	C 1s/1	284.6	1.394	1147.25	36.44	C-C, C=C
	C 1s/2	285.59	2.117	1543.25	49.02	C-O
	C 1s/3	289.26	2.434	457.629	14.54	O-C=O

Although sample 9 was deconvoluted into four synthesis peaks while sample 10 was only into three peaks, both samples showed similar distribution of aliphatic and aromatic C groups, accounting for most of the total C. However, more abundance of mono-oxygenated C was present in sample 9 than sample 10. As for wastewater treatment plant, sample 11, 12 and 13 displayed quite similar characteristics with each other. Their curves were all fitted by three components: underivatized C bond, mono-oxygenated C bond and carboxyl C bond. And mono-oxygenated C (C-O, C-N) took more than 40% of all carbon functional groups, while carboxyl C (O-C=O) took less than 20% of all of those groups. In the freshwater system, the C1s peak in sample 1 was decomposed into all four components as described above. Aliphatic and aromatic carbon is the most abundant component that takes 46.33% of all carbon, while di-oxygenated C and carboxyl C are the secondary and tertiary abundant component, respectively. Sample 2 and 14 have rather similar profiles with three synthesis peaks of components. The main contributions are aliphatic and aromatic carbon (at around 284.60 eV), along with mono-oxygenated carbon (at 285.59-285.86 eV) with a high predominance of the former of 49.02-50.31% (Templier, Miserque et al. 2012).

3.8 Nitrogen functional groups

Fig. 6. showed the high-resolution N1s spectra for all the samples. The spectra were deconvoluted into several Gaussian curves with respective peak centers. By comparing the present measurement results with the reference functional groups from literature data, nitrogen species were mainly classified into three groups: aromatic N including imine, heterocyclic C=N and aromatic amine with peak centers at 399.0±0.1 eV, peptide band N

including other amides, pyrrole, secondary and tertiary amines, and imide with peak centers at 400.4±0.1 eV, and primary amine N including other protonated N with peak centers at 402.3±0.1 eV (Abe, Maie et al. 2005, Maie, Parish et al. 2006). Beside that, there are also some peaks outside this area within the spectra. We assign these peaks as follows: the peak center at 397.2 eV to CH_3CN, the peak center at 398.8 eV to NH_3, the peak center at 403.3-403.7 eV to KNO_2, and the peak center at 407.3-408.0 eV to $NaNO_3$. Table. 7 also showed the principle for nitrogen peak assignment with respect to peak position.

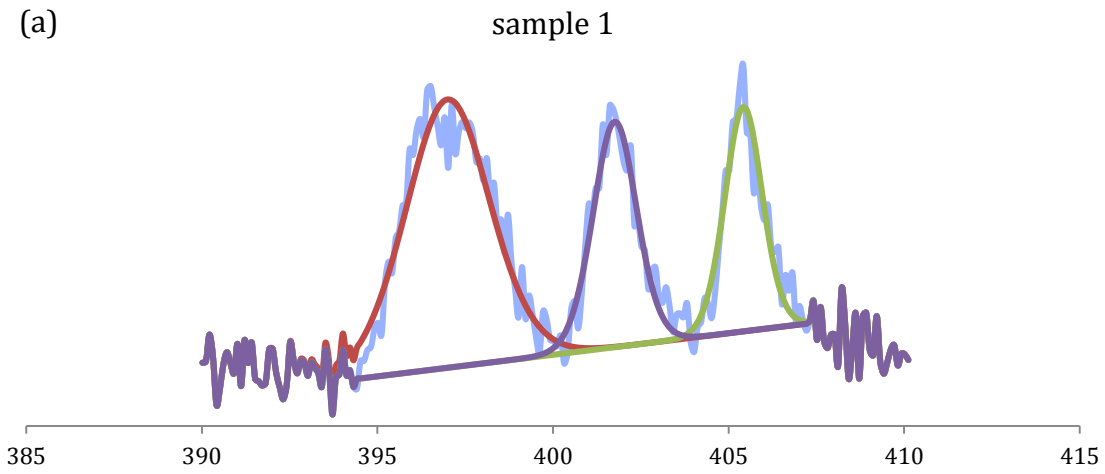

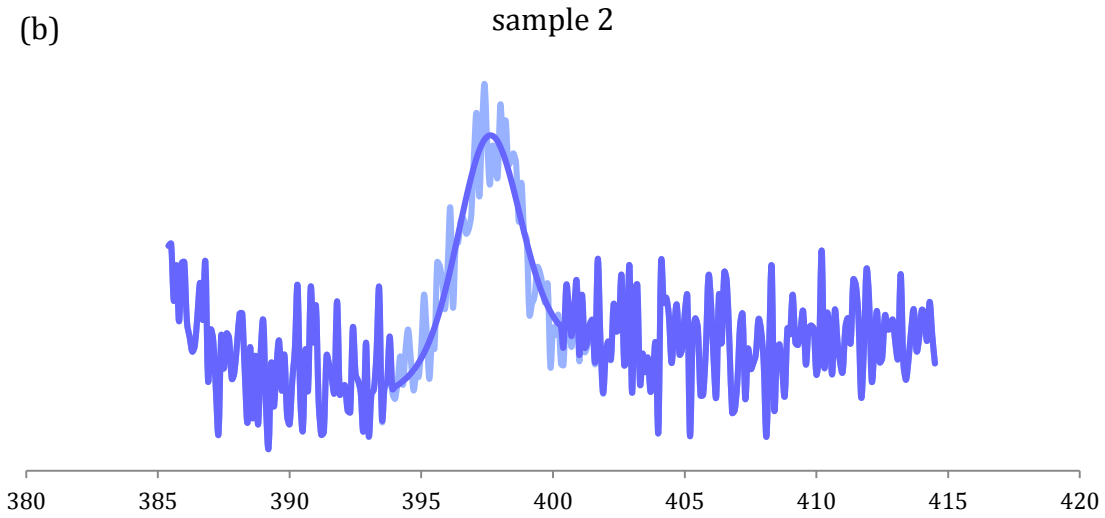

(c)

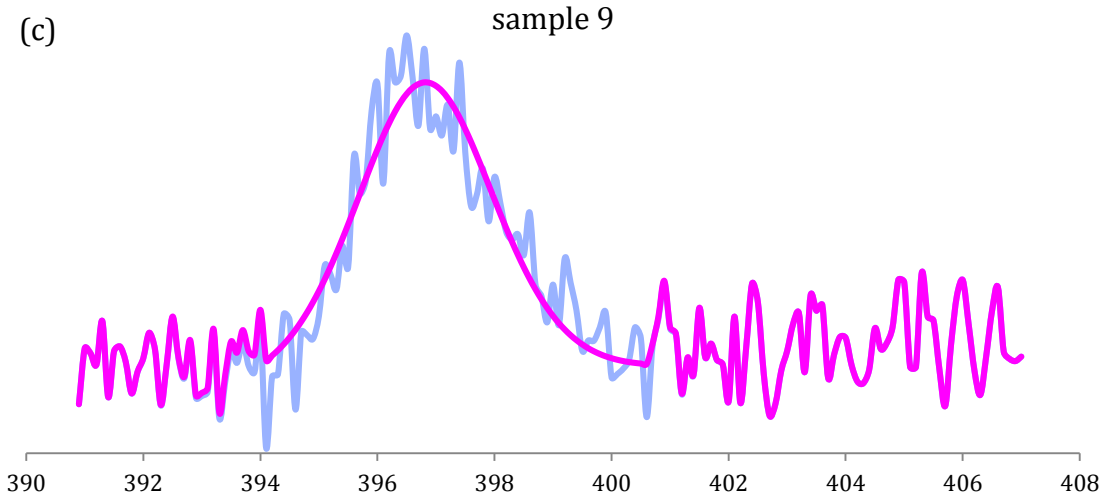
sample 9
390
392
394
396
398
400
402
404
406
408

(d)

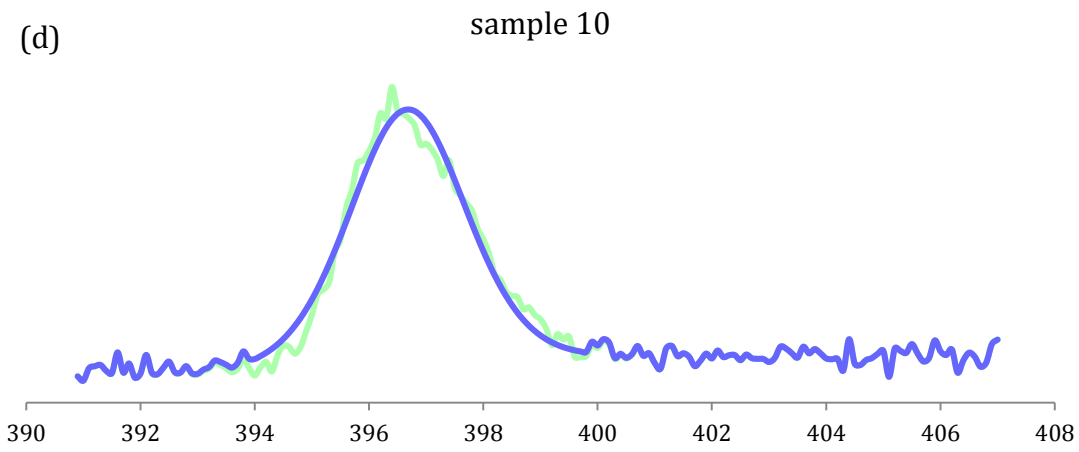
sample 10
390
392
394
396
398
400
402
404
406
408

(e)

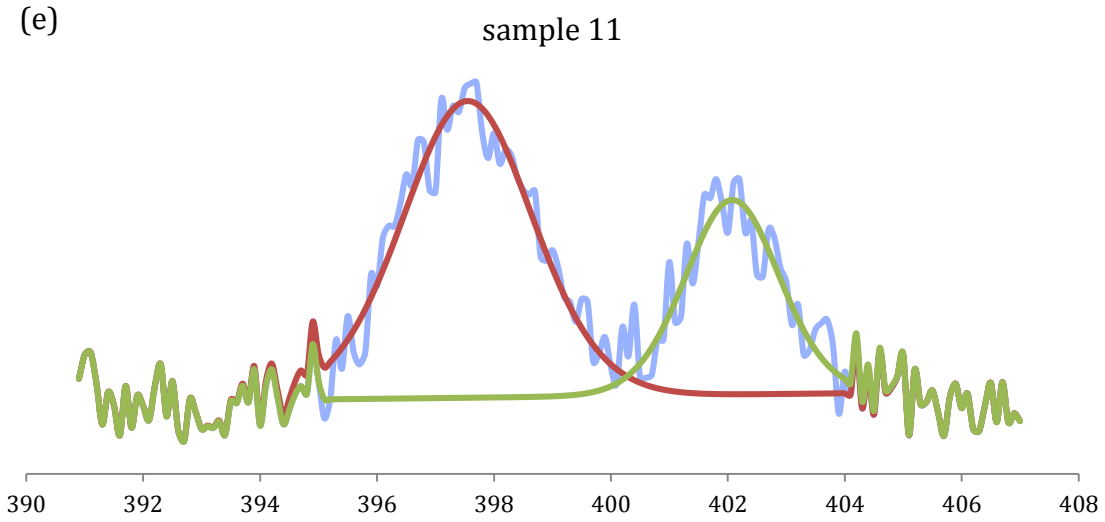
sample 11
390
392
394
396
398
400
402
404
406
408

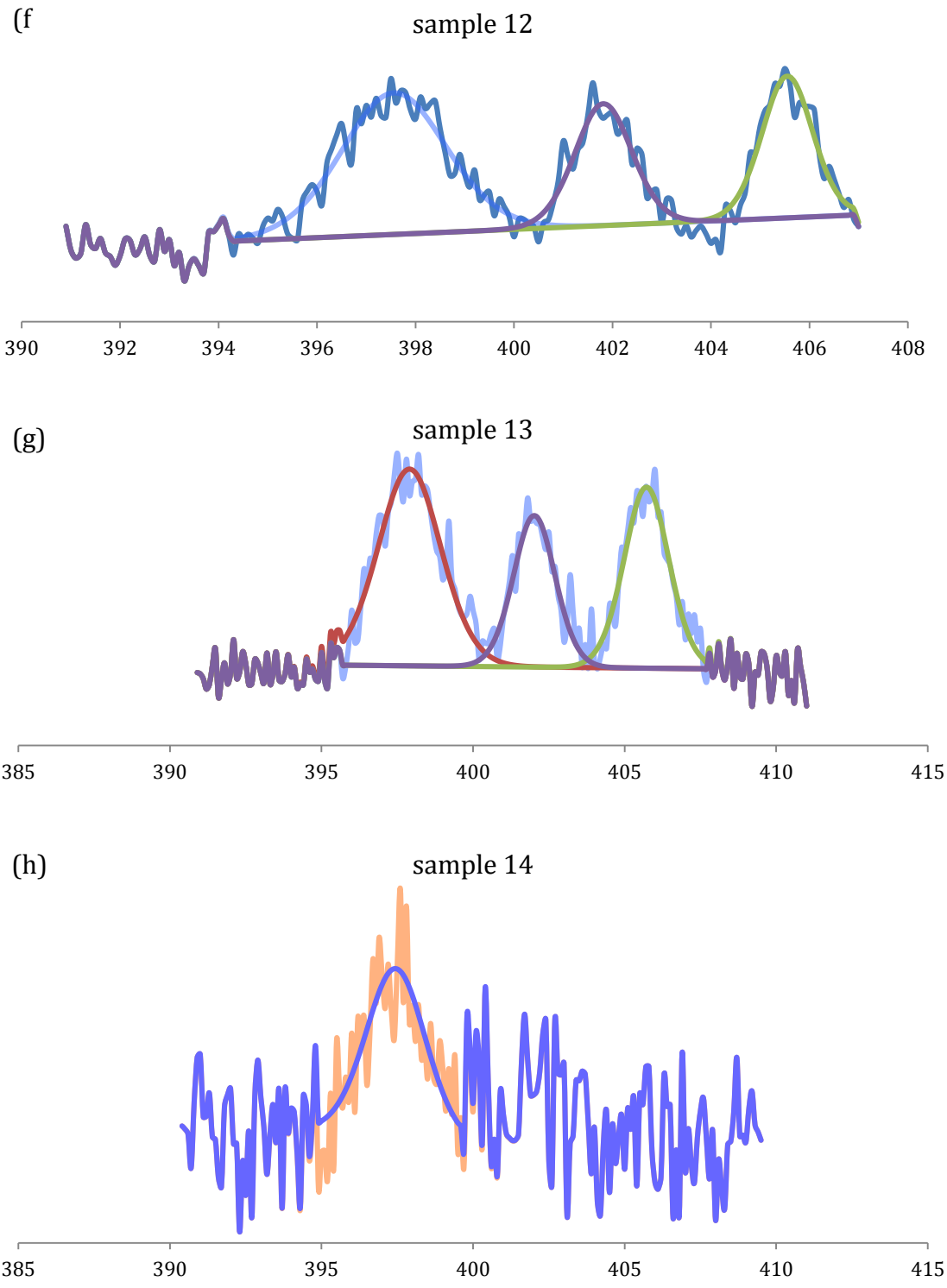

Figure 6 XPS high-resolution N1s spectra of solid samples from different sites: sample 1 (a) and 2 (b) from upstream of Hinkson creek; sample 9 (c) and 10 (d) from city landfill; sample 11 (e), 12(f) and 13 (g) from WWTP; sample 14 (h) from Missouri river. In each sample, light lines are original spectral lines; dark lines are lines of synthesis components.

Table 8 Position, concentration and assignment of synthesis components in XPS N1s high-resolution spectra from each solid sample: sample 1, 2 and 14 from freshwater sources; sample 9 and 10 from city landfill; sample 11, 12, 13 from wastewater treatment plant (WWTP).

Sample ID	Block Id	Position	FWHM	Area/(RSF*T* MFP)	Atomic Concentration	Assignment
1	N 1s/2	397	2.824	126.992	55.36	Aromatic Mixture
	N 1s/2	405.42	1.258	47.1686	20.56	Inoragnic
	N 1s/2	401.76	1.464	55.2163	24.07	Primary
2	N 1s/4	397.58	2.811	116.897	100	Aromatic mixture
9	N 1s/3	396.81	2.749	101.262	100	Aromatic mixture
10	N 1s/2	396.67	2.393	324.867	100	Aromatic mixture
11	N 1s/3	397.55	2.625	118.464	67.78	Aromatic mixture
	N 1s/3	402.08	1.902	56.3102	32.22	Primary
12	N 1s/3	397.56	2.508	101.67	51.27	Aromatic mixture
	N 1s/3	405.55	1.214	49.1293	24.78	Inorganic
	N 1s/3	401.81	1.363	47.5025	23.95	Primary
13	N 1s/3	397.9	2.437	112.386	46.2	Aromatic mixture
	N 1s/3	405.72	1.736	73.5611	30.24	Inorganic
	N 1s/3	402.02	1.616	57.3243	23.56	Primary
14	N 1s/4	397.45	2.327	56.7859	100	Aromatic mixture

Spectra from samples at site 9 and site 10 were both collected from city landfill cells and have many similarities with each other. Only one peak at about 396.7-396.8 eV was observed in each spectrum, which may be considered as a mixture of aromatic N and CH_3CN. The samples from site 11, site 12 and site 13 all basically have two or three peaks at around 397.6-397.9 eV, 401.8-402.1 eV and 405.6-405.7 eV. They are mainly contributions from mixtures of NH_3 and CH_3CN, amines and oxidized N, respectively. The spectrum of sample 1 displays three broad peaks at 397 eV, 401.76 eV and 405.42 eV, which are attributed to –III oxidation state, amine, and oxidized N, respectively. The

spectra for sample 2 and sample 14 both have one peak at around 397.5-397.6 eV, assigned to a mixture of CH_3CN and imides.

The area percentages were calculated and the results are shown in Table. 8. Peaks with lowest binding energy in each spectrum are always in the range from 396.7 eV to 397.6 eV and always has the largest atomic concentration. Peaks in the region of 405.4-405.7 eV occur in spectra for samples 1, 12 and 13, contributing 20-30 percentage of atomic concentration in those samples. Finally, peaks at around 401.8-402.1 eV take 24-32 percentage of atomic concentration in samples 1, 11, 12 and 13.

3.9 Oxygen and Silicon functional groups

Fig.7 displays the representative O1s XPS spectra in the range of 528-536 eV of the original spectra. All of the oxygen signals were deconvolved into four kinds of compounds. The principle oxygen band assignments are found in Table.7. Their binding energy is shown as below: oxygen oxide compounds (A_xO_y) is at 529.4-529.7 eV, the carbonyl oxygen groups (C=O) which included carboxylic acids, carboxylates, ketones and amides is at 531.4-531.5 eV, the hydroxide groups (C-O) which included hydroxyl compounds, acetal and hemiacetal is at 532.1-532.9 eV, and the ester groups (O-C=O) is at around 533.2-534.0 eV. (Fortner, Kim et al. 2007, Wang, Yan et al. 2008) All of our samples contained a large portion of hydroxides or oxide and hydroxide mixtures. Most of them were divided into two synthesis compounds of oxides and hydroxide mixture group and ester group, or three synthesis compounds like oxide and hydroxide mixture group, hydroxyl group and ester group. Sample 1 seemed to be the most complex one with four compounds of oxides,

hydroxides, hydroxyl groups and ester groups. The peak distribution and assignment of each sample were shown in Table. 9.

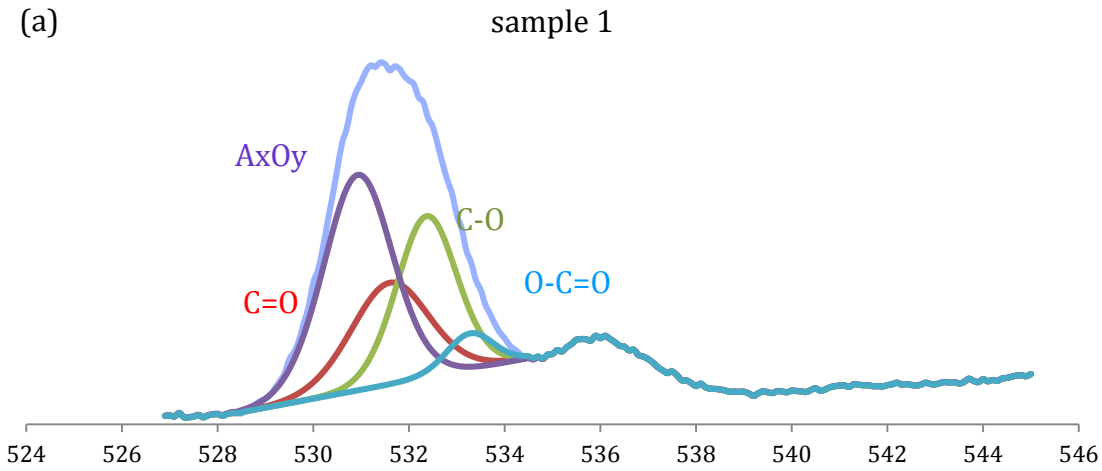

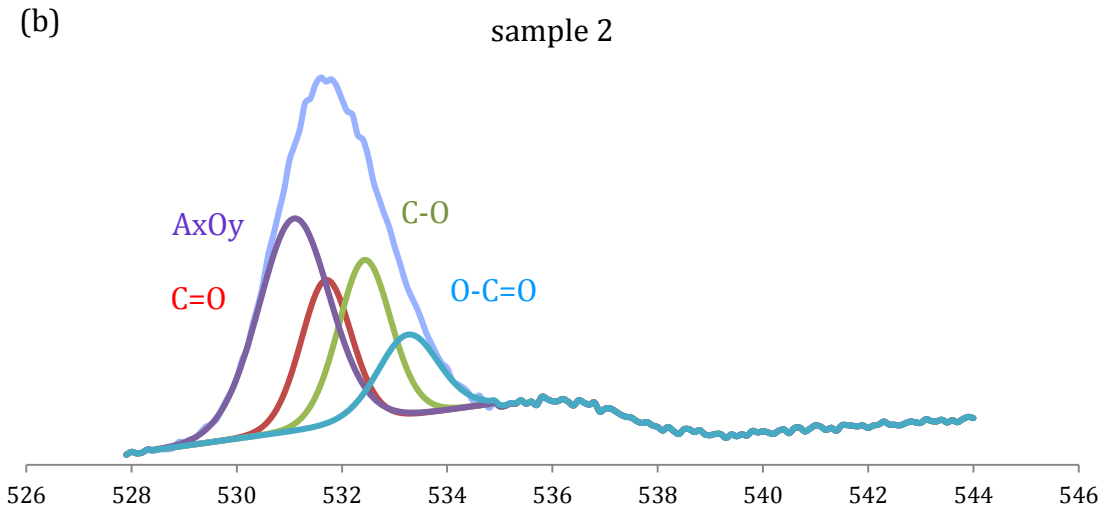

(c) sample 9

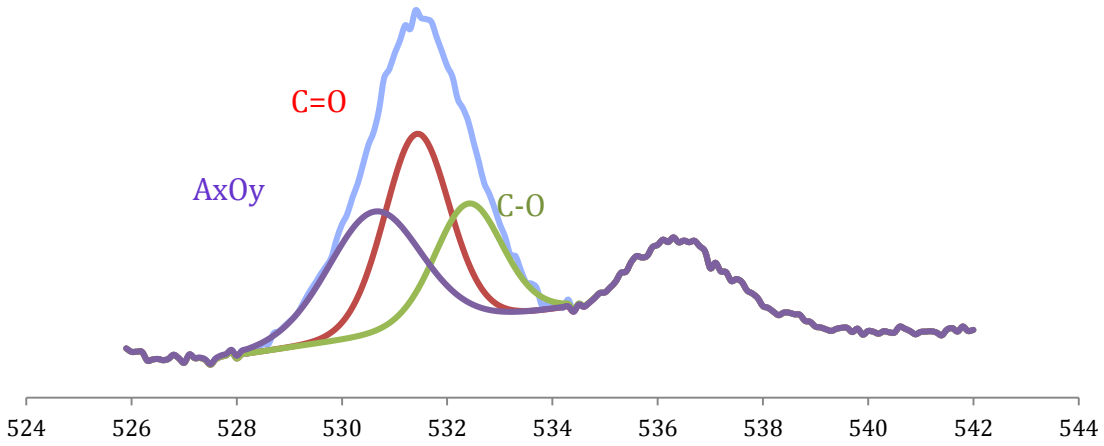

(d) sample 10

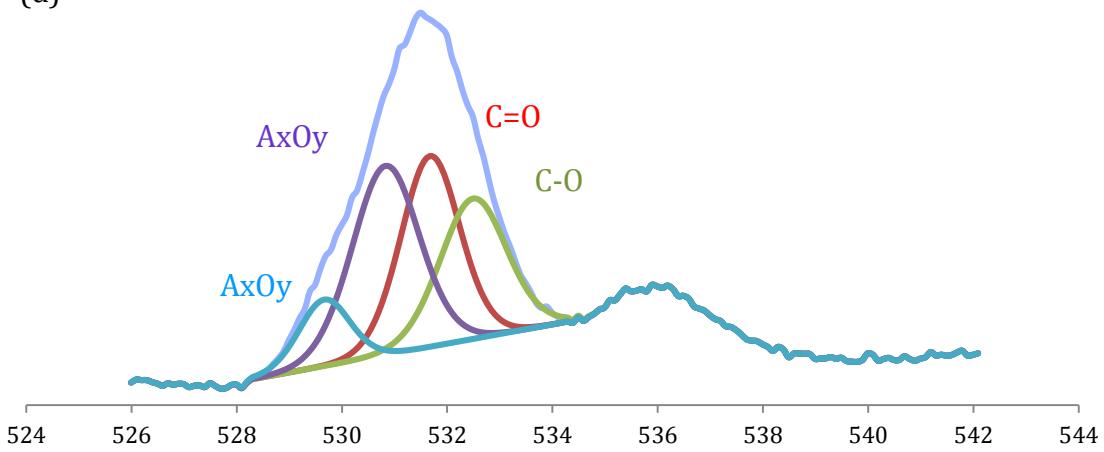

(e) sample 11

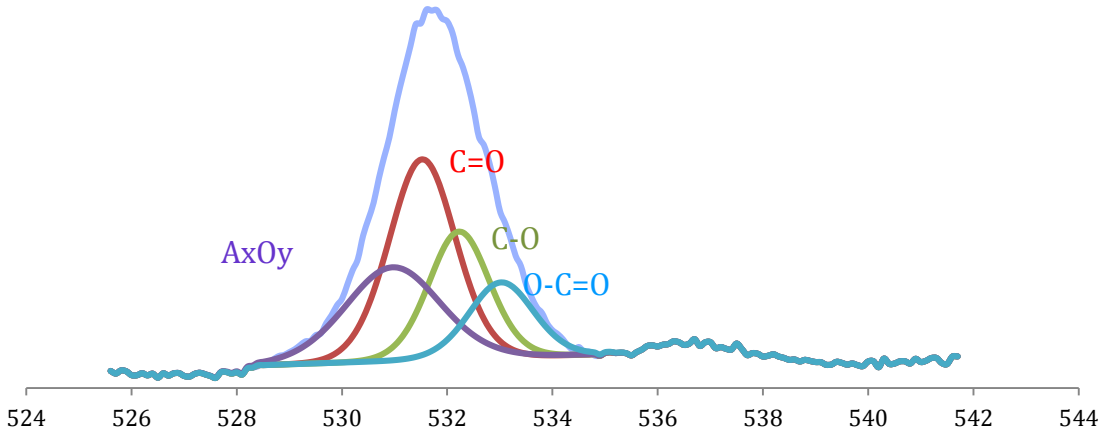

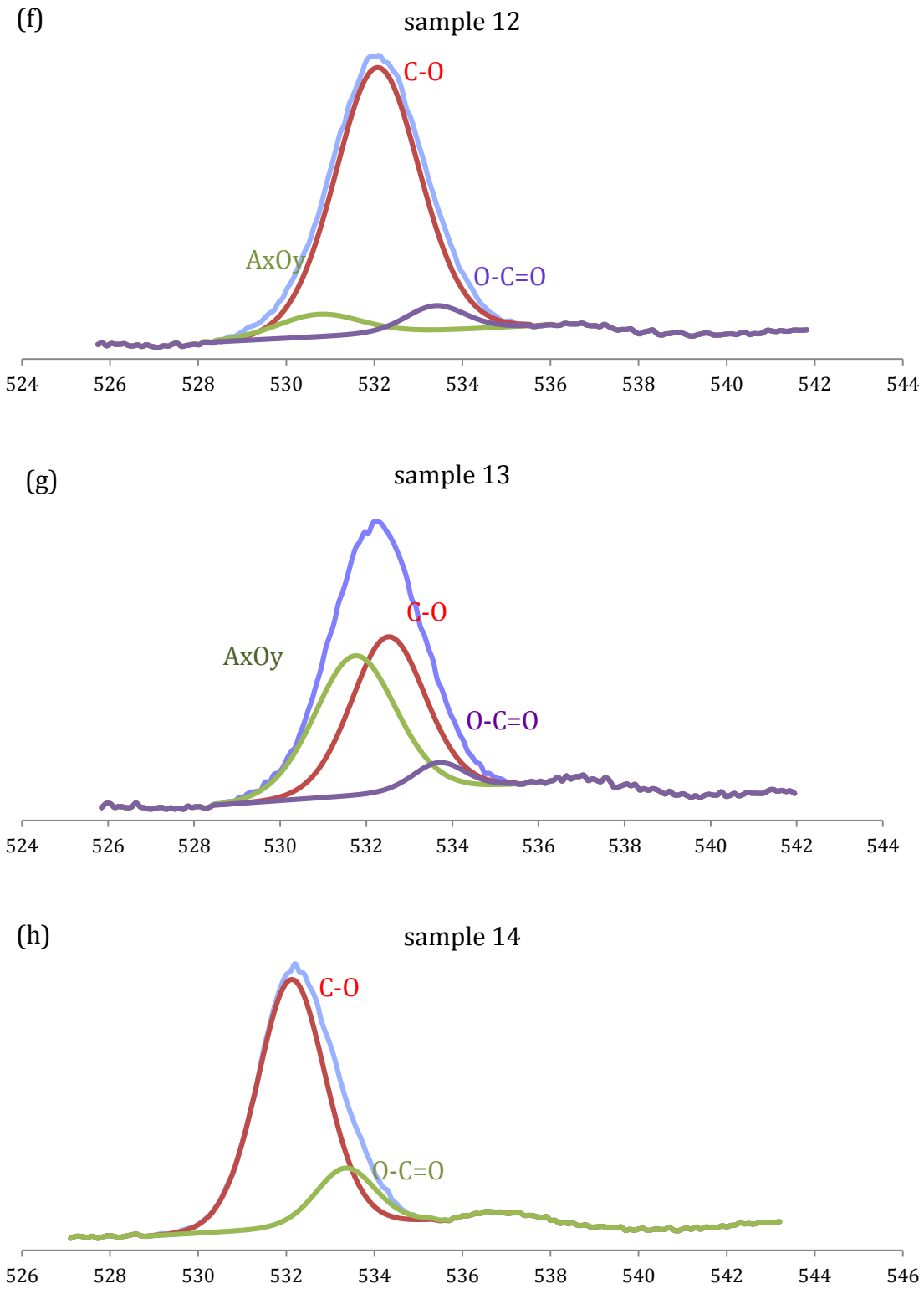

Figure 7 XPS high-resolution O1s spectra of solid samples from different sites: sample 1 (a) and 2 (b) from upstream of Hinkson creek; sample 9 (c) and 10 (d) from city landfill; sample 11 (e), 12(f) and 13 (g) from WWTP; sample 14 (h) from Missouri river. In each sample, light lines are original spectral lines; dark lines are lines of synthesis components

Table 9 Position, concentration and assignment of synthesis components in XPS O1s high-resolution spectra from each solid sample: sample 1, 2 and 14 from freshwater sources; sample 9 and 10 from city landfill; sample 11, 12, 13 from wastewater treatment plant (WWTP).

Sample ID	Block Id	Position	FWHM	Area/(RSF*T* MFP)	Atomic Concentration	Assignment
1	O 1s/1	531.6	1.914	869.329	23.1	C=O
	O 1s/2	532.37	1.483	1068.68	28.39	C-O
	O 1s/3	530.93	1.703	1641.49	43.61	AxOy
	O 1s/4	533.28	1.148	184.174	4.89	O-C=O
2	O 1s/1	531.7	1.131	612.486	20.56	C=O
	O 1s/2	532.43	1.181	704.745	23.66	C-O
	O 1s/3	531.09	1.6	1257.17	42.21	AxOy
	O 1s/4	533.26	1.354	404.027	13.57	O-C=O
9	O 1s/1	531.43	1.459	606.016	39.49	C=O
	O 1s/2	532.41	1.515	379.55	24.73	C-O
	O 1s/3	530.63	2.089	548.905	35.77	AxOy
10	O 1s/1	531.67	1.321	710.234	30.73	C=O
	O 1s/2	532.49	1.488	587.866	25.43	C-O
	O 1s/3	530.83	1.5	799.564	34.59	AxOy
	O 1s/4	529.66	1.14	213.665	9.24	AxOy
11	O 1s/1	531.52	1.487	1320.95	38.4	C=O
	O 1s/2	532.22	1.356	763.376	22.19	C-O
	O 1s/3	530.97	2.116	877.921	25.52	AxOy
	O 1s/4	533.03	1.442	477.434	13.88	O-C=O
12	O 1s/1	532.07	2.259	3212.07	87.03	C-O
	O 1s/2	530.74	2.258	268.064	7.26	AxOy
	O 1s/3	533.39	1.582	210.837	5.71	O-C=O
13	O 1s/1	532.51	2.024	1465.56	47.63	C-O
	O 1s/2	531.74	2.218	1435.1	46.64	C=O
	O 1s/3	533.69	1.418	176.443	5.73	O-C=O
14	O 1s/1	532.12	1.81	4574.81	83.47	C-O
	O 1s/2	533.34	1.578	905.816	16.53	O-C=O

From the XPS O1s high resolution spectra, a nearly steady distribution (about 24-28%) of mono-oxygenated and hydroxyl carbon (C-O, C-O-H) was found in sample from sites 1, 2, 9 and 10 and such distribution mostly increased but varied a lot in the rest of the samples. High predominance of organometallic oxides were indicated in samples from site 1 and 2 that takes more than 40% of the oxygen-containing composition. This contribution reduced since the water across down gradient to the Missouri river.

Fig. 8 displays the Si 2p XPS spectra from sample 2 and sample 14 because of their relatively abundant concentration of silicon. The silicon signal in sample 2 was only divided into one compound with the intensity at 100.66 eV. The position of 100.66 eV is always assigned to saline or silicide combined with carbide, benzene and nitride. In the sample 14, the signal was decomposed into two signals at 100.8 eV and 102.1 eV, respectively, which were mostly attributed to silicon-contained organometallic, benzene, nitride and hydrate.

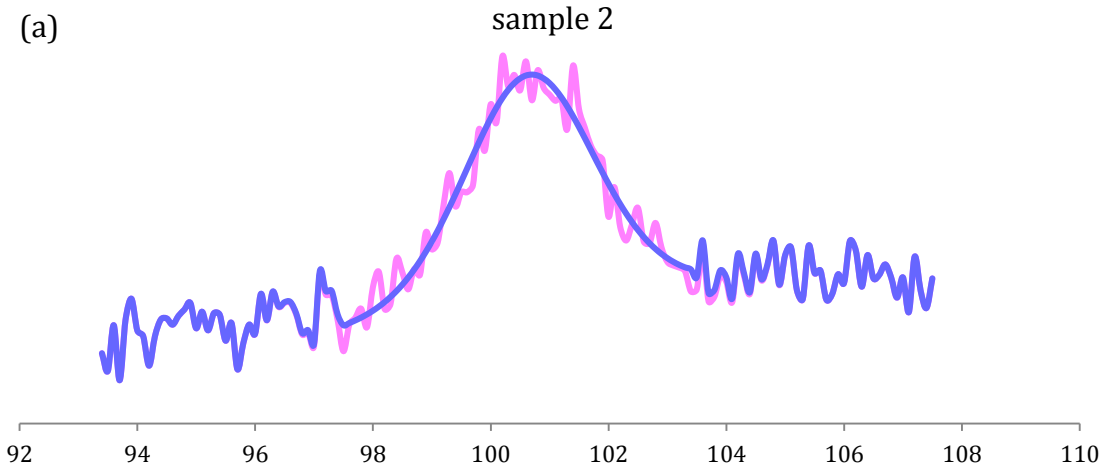

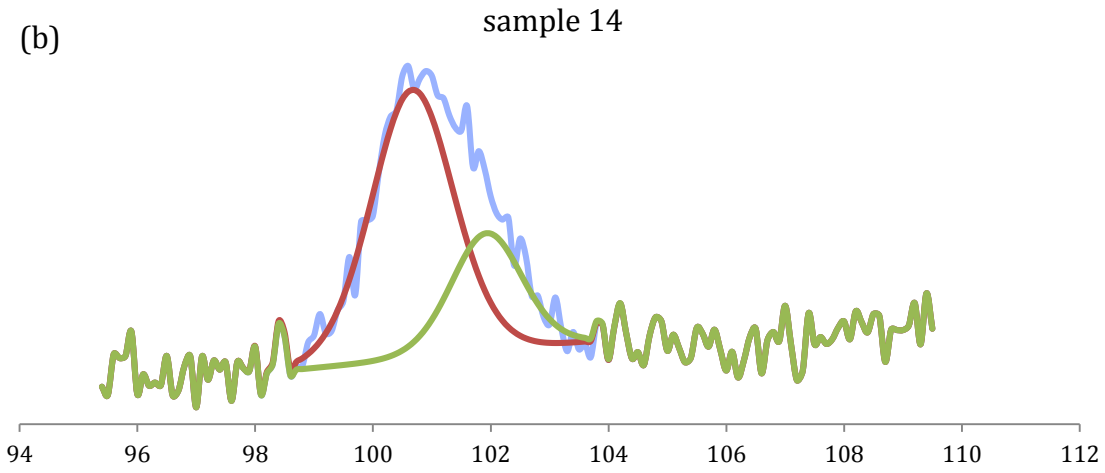

Figure 8 XPS high-resolution Si2p spectra of solid samples from different sites: sample 2 (a) from upstream of Hinkson creek; sample 14 (b) from Missouri river. In each sample, light lines are original spectral lines; dark lines are lines of synthesis components

3.10 Summary

From wide-scan spectra of eight solid samples, we obtained atomic composition and elemental ratios as shown in Table. 4 and Table. 5, respectively. Carbon and oxygen account for the largest proportions of all element fractions. Sample from landfill cells had the greatest concentration of carbon and the corresponding low O/C and N/C ratio. This indicated abundant aromatic and aliphatic groups contained in landfill leachates. As for samples from WWTP, the concentration of oxygen and nitrogen increased significantly. High O/C was also found in such samples, which demonstrated carbohydrate and other oxygen-contained components contributed the most part of DOM fractions. In freshwater system, samples from different sources showed much diversity with each other. Sample 1 and 2 both presented high oxygen concentration, but sample 2 had an extremely high concentration of carbon. As a result of that, O/C ratio was quite low in sample 2. However, N/C ratio was almost the same, which indicated a relatively high concentration of nitrogen

in sample 2. We can conclude that site 2 might contain more aromatic-like groups while both sites had abundant oxygen-containing groups. When it comes to sample 14 from the Missouri river, those parameters again showed great diversity. Oxygen concentration was extremely high but nitrogen concentration decreased. The phenomena may be due to Missouri river receiving multiple effluents from various sources, which accumulated specific elements and functional groups.

The peak identification of carbon, nitrogen and oxygen in high-resolution spectra are shown in Table 7, Table 8 and Table 9. According to these tables, characteristics of samples from different sources were compared. Carbon distribution was similar in samples from WWTP and Missouri river. Carbohydrate-like components contributed the largest fraction that resulted from high concentration of C-O bands identified by peak model fitting. In sample 9 and 10, abundant aliphatic and aromatic carbon was found with the percentage of 50%-70%. Carbon peak models still vary a lot between sample 1 and 2. A high concentration of C-O band was present in sample 2 while four kinds of carbon bands all appeared in sample 1. As for nitrogen distribution, samples from landfill cells only had aromatic-contained mixture. However, multiple components, like primary amine, peptide nitrogen and inorganic groups all appeared in synthesis peak models in samples from WWTP. In freshwater system, sample 2 and 14 were relatively alike because of their abundant aromatic nitrogen content, while sample 1 was much complicated with the nitrogen fractions in primary amine and inorganic matters.

CHAPTER 4

Discussion

4.1 Chemical composition features of DOM long the Hinkson Creek observed by FTIR and XPS

Eight samples were collected along the riverine area from upstream of Hinkson creek to the Missouri river. Features were identified for each sample. Combining the results from FTIR and XPS spectra, similarities and differences were compared among the samples. In this part, I would discuss the features of DOM in eight samples and explore the influencing factors that may result in these features.

First, the spectral features of DOM derived from upstream of Hinkson creek (sample 1 and 2) and landfill leachates (sample 9 and 10) were compared. According to FTIR spectra of sample 1 and 2, strong C-(C, H) bands at around 1390-1450cm^{-1} indicated important moieties of aliphatic and aromatic compounds, likely from alkane and lignin-derived products (Templier, Miserque et al. 2012). Beside that, sample 1 showed an aromatic-containing amide band at around 1590cm^{-1} that is likely from proteins with amino acid side chains (Liao, Lin et al. 2011). From XPS high-resolution spectra, sample 1 has high concentration of aliphatic and aromatic bands (about 46%) in the carbon distribution. As for sample 2, the carbon fraction was obviously abundant due to its high concentration (about 44%) and low O/C ratio. A similar observation of aliphatic and aromatic carbon bands was apparent in the samples from the landfill cells (sample 9 and 10). C-H bands are clearly presented at lower (1450cm^{-1}) and higher (2950cm^{-1}) frequencies, respectively.

Aromatic and amide stretches are within the 1580cm^{-1} range as a shoulder on the larger C-(C, H) peak. According to XPS wide-scan data for sample 9 and 10, low O/C and N/C ratio also provided evidence for abundant aliphatic and aromatic carbon fractions. For peak identification, underivatized carbon took nearly 50%-70% of all carbon fractions in both samples.

The DOM samples from Hinkson creek (sample 1 and 2) and landfill leachates (sample 9 and 10) all had characteristics in consistent with abundant aliphatic and aromatic functional groups. Especially in samples 9 and 10, both FTIR and XPS data showed consistent evidence that aromatic and aliphatic components were the largest fraction of DOM. Weak oxygen and nitrogen-containing signals were found in these two samples. The aromatic groups often refer to refractory organic matter affected by riverine sediment (Stephens and Minor 2010). However, when it comes to sample 1 and 2, even if large underivatized carbon was contained, they had diversity in elemental and functional distribution. For example, sample 1 showed high concentrations of oxygen proved by a large oxygen fraction in the atomic composition and high O/C ratio. Sample 2 presented abundant C-O bands in carbon distribution and a strong nitrogen signal. These features will be discussed later.

Second, the features of DOM derived from the wastewater treatment plant (sample 11-13) and Missouri river (sample 14) were identified. In the FTIR spectra of these four samples, strong and multiple C-O bands appeared at around 1030cm^{-1} while the intensities of C-H bonds decreased sharply. A clear band at around 1650cm^{-1} emerged in each spectrum respectively, which was assigned to C=O band of esters and amides. From the XPS wide-

scan data, high O/C and N/C ratio was found in samples from the WWTP (sample 11-13). High C-O band concentration (about 42-47%) and multiple kinds of nitrogen bands were indicated by peak identification. As for sample 14 from the Missouri river, similar features, such as high O/C ratio and large C-O band fraction (49%), were also found by XPS technique. However, there were some differences occurred that in the concentration and distribution of nitrogen-containing groups among these samples.

There is a likelihood that the C-O groups, which come primarily from alcohol, carboxylate and carbohydrate, are dominant in DOM fraction in the effluent of WWTP and Missouri river (Matamoros and Salvadó 2012). The strong C-O bands in the FTIR spectra also showed a significant signal of polysaccharides that contain phenolic, acetal and hemiacetal distribution in samples 11-14 (Liao, Lin et al. 2011). Beside that, there was an increase of amide and acid groups own to the stronger peaks at 1650cm^{-1} and stronger signals from oxygen and nitrogen. Amides primarily referring to protein and nitrogen functionalities differ depending on the sources of organic matter(Hwang and Li 2010). Comparing the samples from WWTP and Missouri river, nitrogen-containing groups showed the most diversity. High concentration of nitrogen was found in samples from the WWTP with a loss of aromatic structure and an increase of primary and oxidized nitrogen. On the contrary, weak nitrogen signals appeared in sample 14 with aromatic-containing mixture as the single type of component (Provenzano, Caricasole et al. 2010, Wu, Tang et al. 2011).

In conclusion, DOM in the eight samples along the river run (from site 1 to 14) shows a decreasing trend in the proportion of aliphatic and aromatic groups, and an increasing

trend of C-O containing components as well as amide and acid groups. Moreover, samples from non-point sources (Hinkson creek and Missouri river) showed many diverse features, especially in oxygen and nitrogen distributions; while samples from point sources (landfill and WWTP) were quite similar with each other in terms of spectral line shape, elemental ratio and functional groups distribution.

4.2 Riverine DOM characteristic affected by land use in non-point sources

Although two tributaries of Hinkson Creek (site 1 and 2) are adjacent to each other under similar climate and soil condition, they a in the features of DOM. The reason for this diversity was likely due to various land use. In this part, I would discuss the characteristics of DOM in sample 1 and 2, and compare the sources of DOM input from two sample sites and their impact on the surrounding environment.

First of all, the distribution of C=O band containing groups, like carboxylic, ester and amide, was explored in the two samples. From the FTIR spectra, we found sample 1 has more complexity in its basic shape. The aromatic and amide stretches (1590cm^{-1}) and stronger carboxylic bond (1790cm^{-1}) were both observed in site 1 but not in site 2. The second derivative spectra from the two sample sites is shown in fig. 9, indicating vibrational modes in corresponding regions for amide, carboxylic and ester groups. From the assignment of peaks shown in Table. 10, amide bands were found at 1649, 1548, 1267 cm^{-1} in sample 1, which are more than such bands found in sample 2. As for carboxylic groups, bands of de-protonated carboxyl group (COO^-) and carboxylic acid (COOH) were

intense and abundant in both sites. When it comes to ester groups, abundant ester bands at 1768cm^{-1}, 1732 cm^{-1}, 1176 cm^{-1} and 1068 cm^{-1} respectively appeared in the spectrum of sample 2, indicating ester groups largely exist in site 2 including aliphatic ester, oxygen-contained chain and lactone. However, some specific structures of ester were lacking in the spectrum of sample 1. From the XPS study, we found almost equal concentrations of oxygen appeared in two samples. By peak identification, carbonyl carbon (C=O) and carboxylic carbon (O-C=O) took slightly higher percentage in sample 1 than in sample 2. Beside that, more complex types of nitrogen were identified in sample 1 even if its nitrogen concentration was relatively low.

As a result, amide was relatively abundant in sample 1, while ester groups contributed more in sample 2. In both samples, terrestrial DOM emerged in terms of various C=O containing components and with strong signals. The more complex the structure of terrestrial DOM was, the greater terrestrial features it showed(Zhang, Yang et al. 2013). The terrestrial features that are related to amino acid or organic acid contributed a lot to the low molecular weight DOM fraction. However in site 2, aliphatic and ring esters at significant amounts are mostly from lipid compounds and display a large proportion of high molecular weight DOM. They may be enriched by runoff input of humic substance coming from forest litter and marsh inputs or swamp organic matters (Minor and Stephens 2008, Abdulla, Minor et al. 2010). There was a significant loss of lipid structure of DOM in site 1 that may be a result from the agricultural land use and human activities. Secondly, the C-O and O-H bands were identified in order to figure out the carbohydrate distribution in the two tributaries. In the FTIR spectrum of sample 2, as described in the

Table 10 Peak position and assignment of each compound class in secondary derivative FTIR spectra of each soild samples: sample 1, 2 and 14 from freshwater sources; sample 9 and 10 from city landfill; sample 11, 12 and 13 from wastewater treatment plant (WWTP).

Compound class	Type	Assignment	Standard band position	Band position in sample							
				1	2	9	10	11	12	13	14
Carboxylic acid		C=O stretch	1710±15	1695	1712	1712	1712	1695, 1712	1695, 1711	1711	1697, 1714
		C-O stretch	1265±55	1267	1265	1261	1261	1271	1270	None	1266
	COOH	O-H bend inplane	1418±22	1413	1410	1400	1412	1402	1402, 1432	1402	1408, 1421
	COO-	Asymmestric stretch	1600±40	1562, 1603	1569, 1629	1591, 1620	1595, 1614	1568, 1639	1620, 1639	1620	1576, 1626
		Symmertic stretch	1405±45	1383, 1415	1379, 1439	1400, 1442	1379, 1412	1383, 1402	1383, 1402	1383, 1402	1385, 1408
Ester		C=O stretch	1740±10	1732	1743	1728, 1745	1728, 1743	1728, 1745	1728, 1745	1728, 1745	1732, 1747
		C-C-O stretch	1185±25	None	1176	1185	1184	None	None	None	1190
	Aliphatic	O-C-C stretch	1065±35	1039, 1095	1068	1047, 1074, 1097	1051, 1097	1070	1051, 1081	1051, 1080	1038, 1059, 1084
	Acetyl	C-C-O stretch	1240±5	None	None	1238	1245	None	None	None	1243
	Lactones	C=O stretch	1770±10	1766	1768	1768	1768	1770	1764	1765	1760
Amide		Amide-1 C=O stretch	1650	1649	1647	1646	1654	1648	1639, 1662	1639, 1664	1637, 1658
		Amide-2 C=O stretch	1550	1548, 1562	1554	1554	1552	1552	1558	1554	1544
		Amide-3 C=O stretch	1260±40	1267	None	1261	1261	1271	None	None	1265
Carbohydrate		C-O asymmetric stretch	1100±100	1095, 1109	1068, 1109, 1157	1030, 1047, 1097, 1157	1051, 1097, 1122, 1155	1070, 1083	1081,1137, 1174	1080,1140, 1174	1059, 1084, 1117, 1153
		O-H bend inplane	1350±50	1352	1363, 1379	1361	1379	1326, 1383	1351, 1383	1349, 1383	1340, 1385
Lignin	Ar-OH	C-O asymmetric stretch	1230±30	None	None	1203, 1261	1232, 1261	None	None	1216	1212, 1228
	Ar-lignin	Aromatic ring vibration	1515±5	1516	1516	1516	1516	1517	1517	1517	1509, 1521
Paraffin		CH2 deformation	1450±10	1450	1439	1442	1448	1440	1450	1450	1446
	Aliphatic	CH3 asymmetric deformation	1460±10	1465	1468	1460	1463	1467	1467	1467	1459
		CH3 umbrella mode	1375±10	None	1379	1376	1379	1383	1383	1383	1385
	Acetyl	CH3 symmetric bend	1430±5	None	None	None	None	None	1435	1430	1432

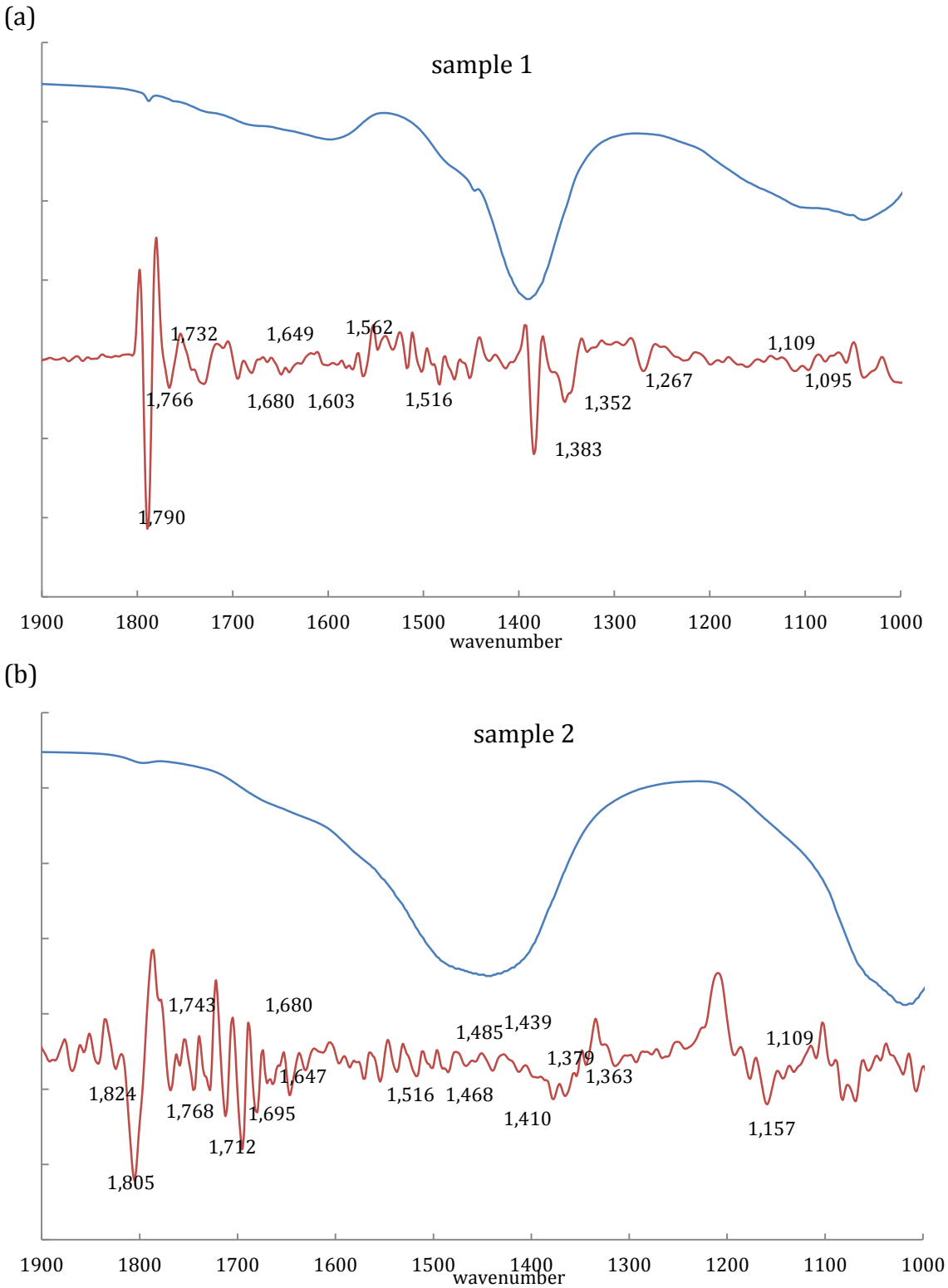

Figure 9 FTIR original (upper) and secondary derivative (lower) spectra of solid samples from different sites: sample 1 (a) and 2 (b) from two upstream of Hinkson creek.

previous part, the peak at 1030cm^{-1}, which was assigned to C-O vibrational stretch of carbohydrate, was much stronger than such peak in sample 1. In the secondary derivative spectra, in-plane bending of O-H vibration of carbohydrate were found in two spectra at 1352cm^{-1} and at 1363cm^{-1}. However obviously more bands assigned to C-O stretch occurred in the range of 1000-1100cm^{-1} in site 2. In accordance with that, XPS C1s high-resolution spectra indicated mono-oxygenated carbon (C-O) accounted for 50% of all carbon in site 2, much higher than the proportion in site 1.

These conditions implied carbohydrate is the major component of low molecular weight DOM in sample 2. Carbohydrates are bioactive and play a critical role in ecosystems, serving as a major structural component for planktonic cells and as an energy transportation medium for heterotrophic metabolism (Wang, Cai et al. 2013). Multiple sources are possible for carbohydrate production, such as mixing of terrestrial organic matter from tributaries, organic degradation and removal processing, and so on (Kaiser, Simpson et al. 2003). The high concentration of carbohydrate in forest-covered land (site 2) mostly originated from the leaching of plant litter and organic-matter-rich soils. Compared with site 2, the input of allochthonous DOM to cropland (site 1) was limited by its less productive agricultural cropland and basin. Human activities heavily influenced the nutrient loading and land cover change, which spurred plankton production and microbial respiration of organic carbon in addition to enhancing photochemical degradation. In addition, water residence time along the tributary in site 1 may be another reason that results in a rapid recycling and removing rate of terrestrial DOM and most of terrestrial

carbohydrate could be lost or recycled along the riverine regions (Abdulla, Minor et al. 2010, Wang, Cai et al. 2013).

Finally, as for lignin and paraffin compounds (with typical aromatic and aliphatic functional groups, respectively), both sites presented similar characteristics. In the secondary derivative spectra of two samples, C-O asymmetric bands of phenol compounds appeared at around 1109cm^{-1}, while the aromatic ring vibrations at 1516cm^{-1} were also found. From the wide-scan XPS spectra, sample 2 showed a much higher carbon and nitrogen concentration. And aromatic mixtures were the main distribution of nitrogen. We can conclude that lignin existed in both tributaries while site 2 had relatively more abundant aromatic groups. Lignin in DOM is isotopically lighter and difficult to be utilized by microorganisms than carbohydrate(Landry and Tremblay 2012). However, lignin is more susceptible to photo-oxidation than carbohydrate, which can be remineralized to dissolved inorganic carbon in remaining DOM (Zhang, Du et al. 2013). The strong paraffin vibration shows that aliphatic compounds existed at a significant concentration in DOM regardless of the land uses, indicated by specific bands from two samples at 1450 cm^{-1}, 1460 cm^{-1} assigned to CH_2 and CH_3 deformation, respectively. XPS carbon identification also showed steady paraffin composition in both sites through their steady contribution of C- (C, H) bands.

4.3 DOM characteristic affected by treatment process in point sources

Landfill and wastewater treatment plants (WWTP) were the two main point sources examined in this study. Landfill leachates are the primary process for municipal solid

waste disposal and are generally characterized as a complex recalcitrant wastewater containing high concentration of dissolved organic matter (Bu, Wang et al. 2010). DOM accounts for more than 85% of the organic matter in terms of dissolved organic carbon and is always the major component of leachate treatment (Xi, He et al. 2012). WWTP receives complex mixtures of urban and industrialized discharges (Zhang, Qu et al. 2009). Dissolved organic matters come from domestic and industrial urban sewage and constitute a key component of the carbon cycle controlling the speciation and bioavailability of trace contaminants. In this part, I would discuss features of DOM and its corresponding point sources and explore the interaction between DOM and its surroundings.

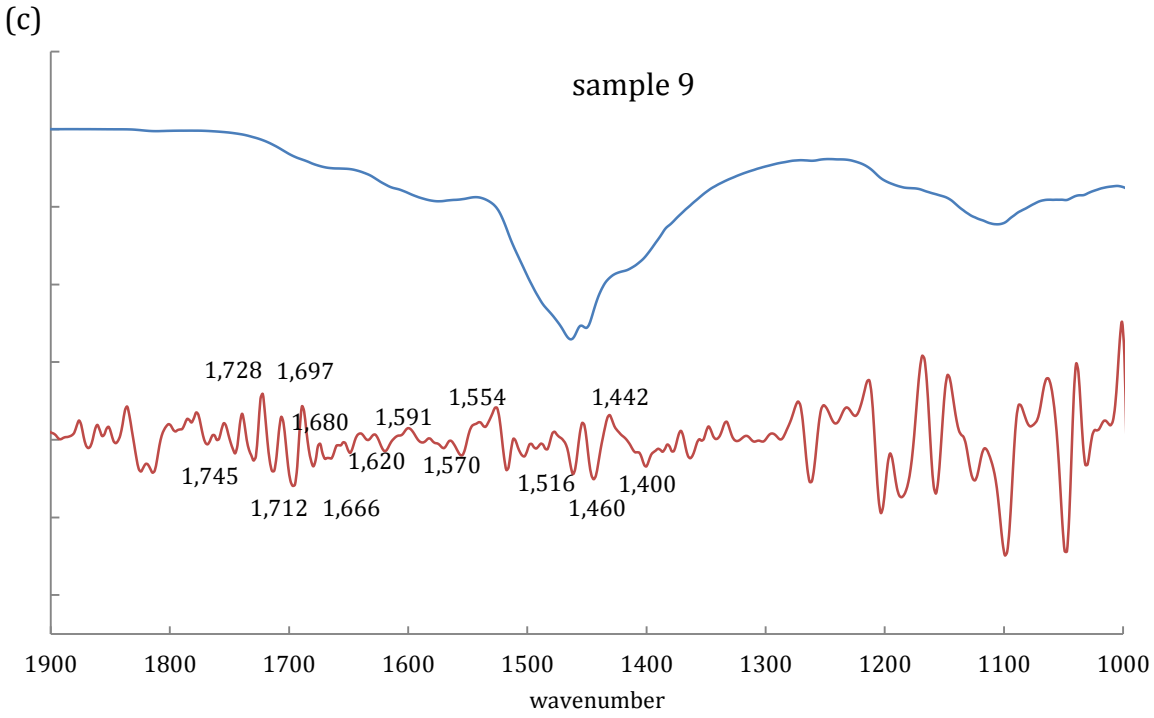

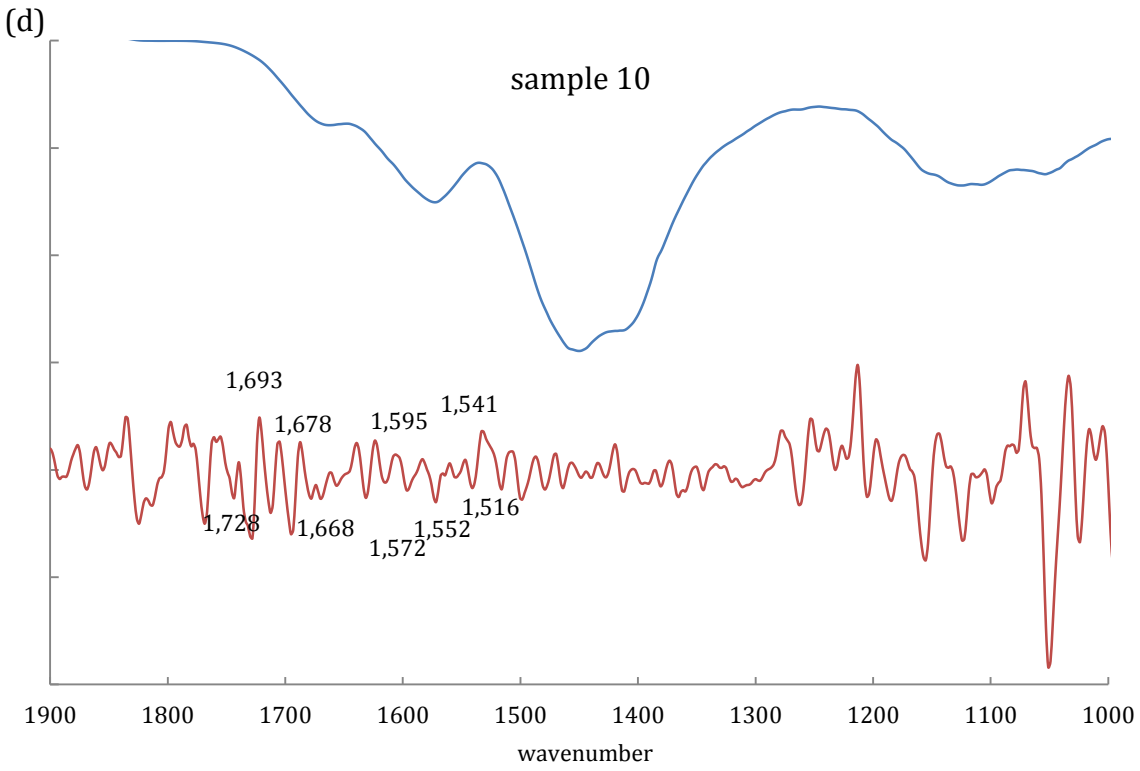

Figure 10 FTIR original (upper) and secondary derivative (lower) spectra of solid samples from different sites: sample 9 (c) and 10 (d) from two city landfill leachates.

Looking at the FTIR spectra of landfill samples (sample 9 and 10), the most obvious observation was the bands at around 2950cm^{-1} and 1450cm^{-1}, which illustrated the presence of hydrocarbons like methyl, methylene and aliphatic C-H in these two samples as described previously. In the range of 1500-1700cm^{-1}, we took advantage of the second derivative spectra shown in Fig. 10 from both sites to explore the distribution of amide and aromatic groups. In the spectrum for sample 9, the signals at 1554 and 1570cm^{-1}, which were attributed to N-H bending of secondary amide groups, as well as bands at 1666 and 1680cm^{-1} owing to the C=O stretch of first amide groups. Similar signals were found in the spectrum for sample 10, showing the parallel amide distribution in both landfill cells. The absorbance bands at 1591cm^{-1} in sample 9 and 1595cm^{-1} in sample 10

were assigned to the aromatic groups. XPS data indicated a low concentration of nitrogen, mostly distributed as an aromatic mixture, in both samples. A low O/C ratio implied the low proportion of O-alkyl and carboxylic acids. In accordance with that, underivatized carbon (C-(C, H)) took up 70% of all fractions in carbon distribution shown by high-solution spectra. Lack of nitrogen and oxygen containing substances resulted in a small fraction of hydrophilic organics in leachates(Seo, Kim et al. 2007).

Above all, the first conclusion was that aromatic and aliphatic functional groups were more abundant in leachate samples regardless of different landfill sites (Huo, Xi et al. 2008). Besides, dissolved organic matters in leachate samples were always divided into hydrophobic fractions according to published literatures, like hydrophobic acid, base, neutral (HOA, HOB, HON), and hydrophilic (HIM) fractions (Seo, Kim et al. 2007). Hydrophilic fractions contained fulvic-like acids in addition to humic-like acids, whereas hydrophobic organics contained more protein-like compounds (Zhang, Qu et al. 2009). Sample 9 and 10 contained abundant aromatic or phenolic content along with amide groups that exhibited high intensity of aromatic proteins and are considered similar to hydrophobic acid structures (Bu, Wang et al. 2010, Xue, Zhao et al. 2011). In the early period, organic matters from landfill decomposed by microorganisms and the concentration of DOM was affected by solubilization of readily degradable matters. Protein-like compounds, especially those that are present as free molecules or bound in polypeptide, are unstable and easily utilized by microorganisms. As the landfill time increased, the content of protein-like materials decreased, whereas the content of humic-like substances that are not easily utilized by microbes increased in leachates, and the

degree of humification and stability increased as well (Huo, Xi et al. 2008, Xi, He et al. 2012).

As for samples from the wastewater treatment plant (WWTP), strong C-O bands at 1000-1200cm^{-1} in FTIR spectra clearly indicated the abundance of carbohydrates. We also use secondary derivative spectra shown in Fig. 12 for the overlap area in the range from 1000cm^{-1} to 1900cm^{-1}. Intense vibration at around 1400cm^{-1} was assigned to C-H deformation in aliphatic (Xue, Zhao et al. 2011). N-H bending in secondary amide groups only occurred in site 11, while clear aromatic vibration only appeared in site 13. In the region of 1639-1730cm^{-1}, multiple intense bands appeared in the spectra of all samples, which implied large amount of amide and carboxylic groups. From XPS wide-scan spectra of three samples, the content of underivatized carbon decreased to less than 40% of all carbon fractions, resulting in weak aromaticity in effluents. An increase of C-O containing structure (about 42%-47%) was also identified. In high-solution XPS spectra, high O/C and N/C ratio was found in all samples, implying rich nitrogen and oxygen contents.

(e)

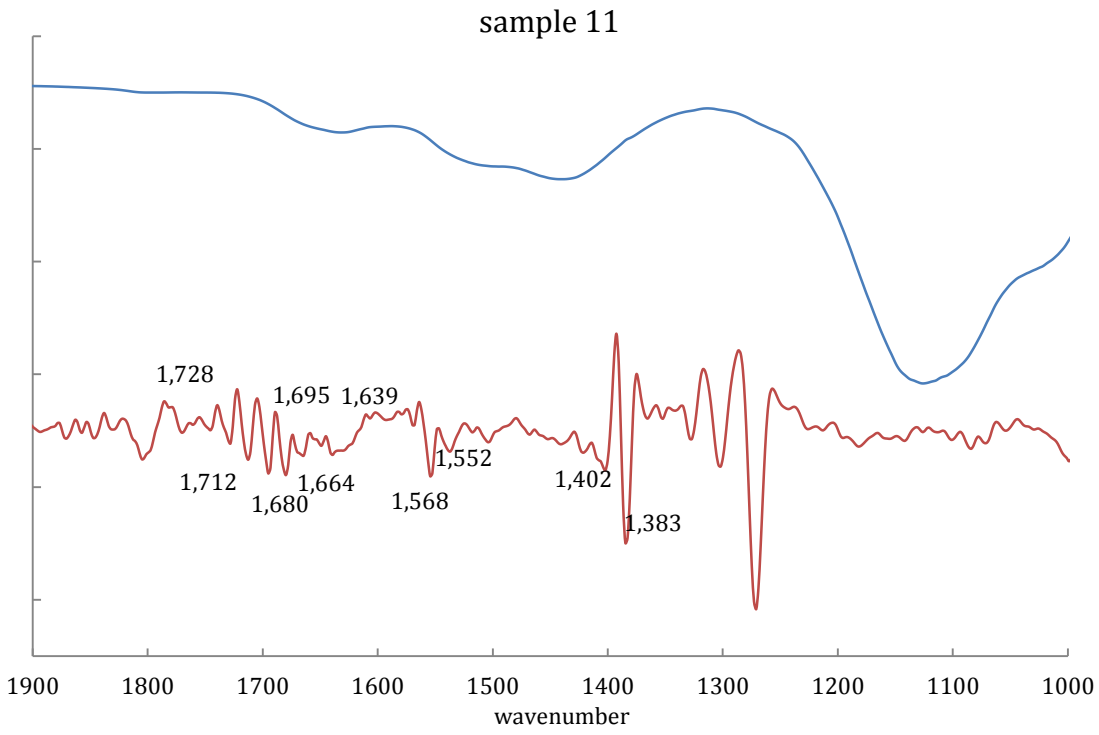
sample 11
1,728
1,695
1,639
1,712
1,680
1,664
1,552
1,568
1,402
1,383
1900
1800
1700
1600
1500
1400
1300
1200
1100
1000
wavenumber

(f)

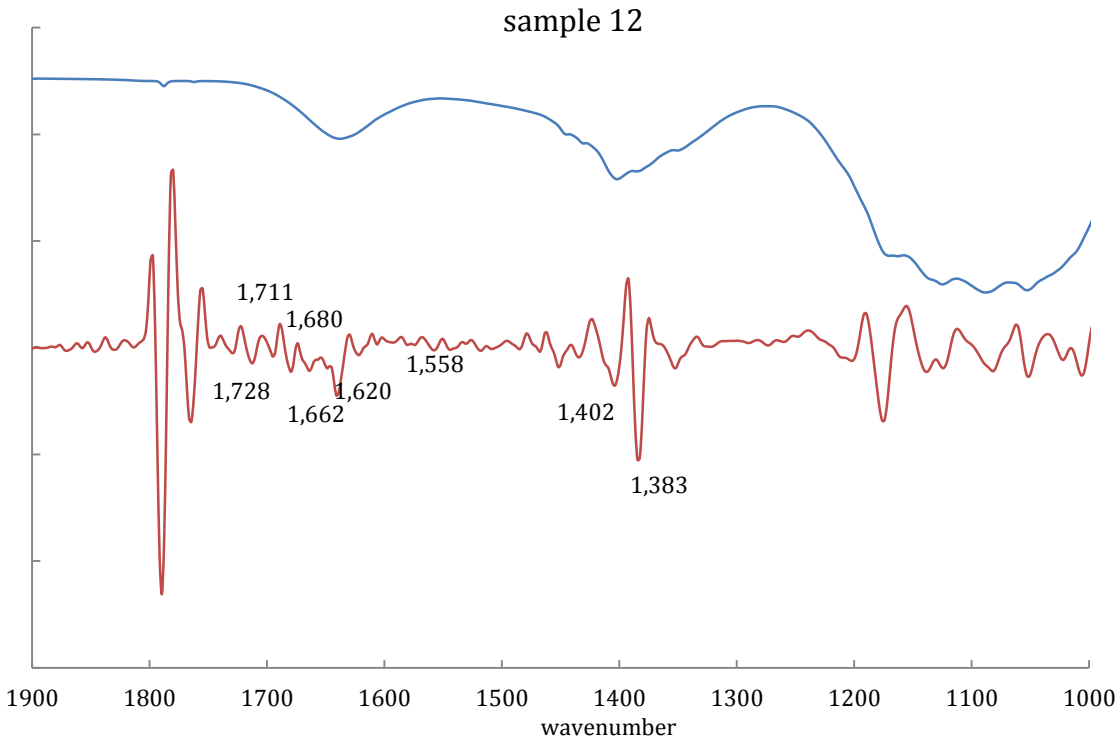
sample 12
1,711
1,680
1,728
1,662
1,620
1,558
1,402
1,383
1900
1800
1700
1600
1500
1400
1300
1200
1100
1000
wavenumber

(g)

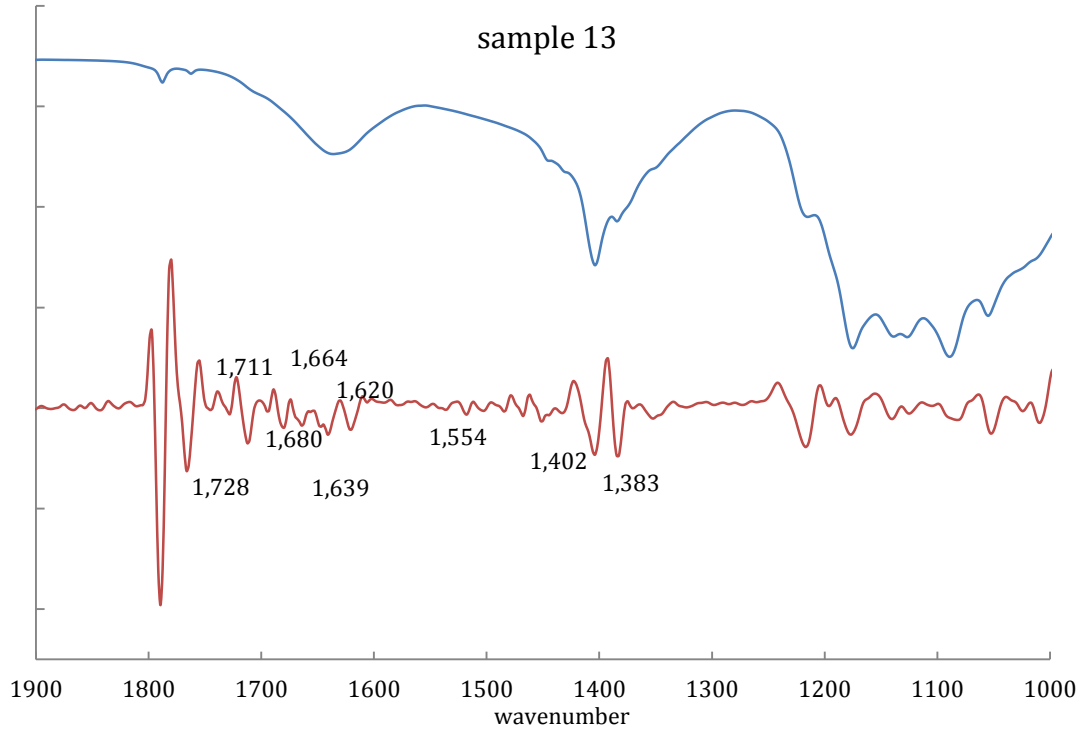

(h)

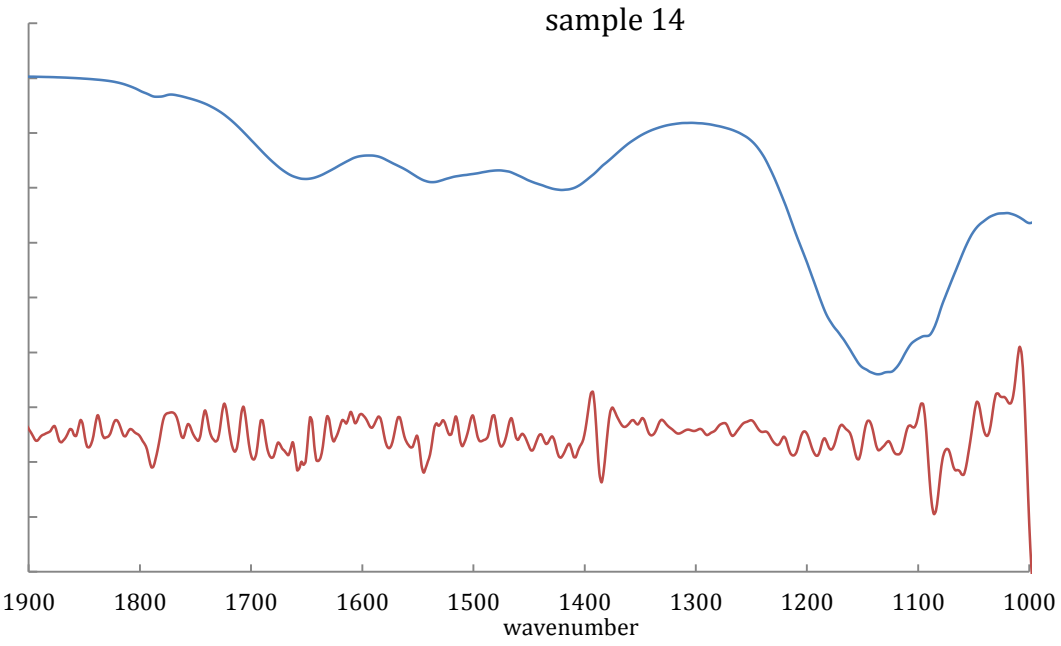

Figure 11 FTIR original (upper) and secondary derivative (lower) spectra of solid samples from different sites: sample 11 (e), 12(f) and 13 (g) from WWTP; sample 14 (h) from Missouri river.

The data demonstrated that DOM in WWTP showed many characteristics of carbohydrates, which are composed of polysaccharides and amino acids (Berman and Bronk 2003). Beside that, the content of carbohydrates and O-alky organics indicated a high concentration of hydrophilic fraction with a small degree of unsaturation and an enrichment in nitrogenized and oxygenated structures (Pernet-coudrier, Clouzot et al. 2008). In other words, poly-sugars and amino acids are important structural components in low molecular weight DOM, while hydrophilic humic-like substance instead of protein-like components predominates in high molecular weight DOM.

As the effluent flew along the WWTP, the Cl/C ratio increased from 0.213 to 0.440, demonstrating the chlorination effect on dissolved organic matters. Both hydrophobic and hydrophilic fractions likely reacted with chlorine, consuming aromatic C=C as well as amide groups and producing C-O, C=O and C-Cl groups. Aromatic groups may easily react with chlorine leading to the formation of disinfection by-products, such as trihalomethanes(Xue, Wang et al. 2009). In this way, chlorination may be one possible reason for the low concentration of aromatic compounds in the effluent. Samples from site 12 and 13 were collected respectively from the inlet and outlet of the constructed wetland, and both samples contained abundant hydrophilic fraction like carbohydrates and carboxylic groups and a strong band for amides related to proteins. There is no distinctive difference of DOM observed between the two sites, except a slight increase of C-O bands and a slight decrease of N/C and O/C ratio indicated by Table. 6 and Table. 7. This difference may be derived from various interactions in the constructed wetland between site 12 and 13, which was located after the secondary wastewater units. Biodegradation,

sorption and photodegradation in the system removed emerging pollutants such as pharmaceuticals to a certain extent. Biomass development, such as the growth of algae and other aquatic plants, enhance the degradation process and accumulate organic matter in the effluent (Matamoros and Salvadó 2012).

4.4 DOM quality in Missouri river affected by point-source input

When quantifying DOM composition in sample 14, we found great similarity with the DOM distribution from the WWTP samples. XPS high-resolution spectra showed similar carbon and nitrogen types and concentrations. Besides, specific functional bands for carboxylic, amide, ester and carbohydrate groups were also found in FTIR secondary derivative spectrum shown in Table. 10. As a primary DOM discharge, the wastewater effluents after final wetland treatment flow into the Missouri river, influencing the DOM composition to a large extent. This may cause the similarity in DOM distribution between the two sites. Moreover, abundant humic substances left in treated wastewater provided large concentration of low molecular weight DOM, like carbohydrate, sugars and acids, and high molecular weight DOM, like protein-like, lipid-like compounds, in the Missouri river. By comparing FTIR spectra from WWTP and Missouri river, more bands of ester groups were obviously presented in sample from the Missouri river, which indicated even higher lipid fractions exist in Missouri river compared to WWTP. This result was also proved by a much higher O/C ratio in sample 14. As being the sum of various DOM-containing tributaries, Missouri river was affected by not only treated wastewater but other sources as well. Freshwater which comes from forest-dominated area always contained abundant lipid components and some of this component left in downstream effluent finally flows

into the Missouri river. Beside that, effluent from landfill leachates may provide acid-like compounds that also contribute to oxygen gathering.

From the table of elemental ratios, we found much lower Cl/C ratio in sample 14, which indicated the chlorination during the treatment process had little effect on downstream water in the Missouri river. This is expected because of dilution effect of Missouri River.

CHAPTER 5

Conclusions

DOMs from point and non-point sources were analyzed by FTIR and XPS spectra to determine their chemical compositions and fractional distribution to DOM. Comparing the two techniques, FTIR has the advantage that one can directly inspect intensities for desired functional groups, providing clear overview of chemical constituents for each sample. XPS was helpful with computing elemental concentration and constructing a synthesis model for specific elements of various binding states. For the riverine DOM, the contribution of carbon-containing and nitrogen-containing compounds in DOM was investigated, and characteristics of each source were correspondingly identified. The sources of DOM inputs, including natural inputs and human activity area, and the aquatic quality was discussed by comparing the land use and treatment processes. With the information carried by DOM features in samples, the relationship between DOM and their corresponding sources were observed. The main conclusions about these characteristics are described as follows:

(1) Generally, riverine DOM among eight sites (from site 1 to 14) showed a strong enrichment of carbohydrate and a weakening proportion of aliphatic and aromatic groups. Land use greatly affected DOM features from non-point sources, while samples from parallel point sources always had similar characteristics within the group.

(2) Abundant carbohydrates and lipid-like components were found in the tributary from a forest-dominated area, resulting from plant leachates and organic matter-rich soils. However, the nutrient loss in cropland caused limited DOM input and showed significant impact from human activities on the surroundings.

(3) Aliphatic and aromatic components were the most abundant fractions in landfill leachates regardless of landfill sites. Additionally, the hydrophobic acid fraction also played an important role even if it would decrease as the time increased by microorganism degradation.

(4) The effluent from the WWTP was rich in carbohydrate, amino acid and hydrophilic fractions. Chlorination and constructed wetland would have an effect on DOM in the WWTP to a certain extent.

REFERENCE

Abdulla, H. A. N., et al. (2010). "Changes in the compound classes of dissolved organic matter along an estuarine transect: A study using FTIR and 13C NMR." Geochimica et Cosmochimica Acta **74**(13): 3815-3838.

Abdulla, H. A. N., et al. (2010). "Using two-dimensional correlations of13C NMR and FTIR to investigate changes in the chemical composition of dissolved organic matter along an estuarine transect." Environmental Science and Technology **44**(21): 8044-8049.

Abe, T., et al. (2005). "Investigation of humic acid N with X-ray photoelectron spectroscopy: Effect of acid hydrolysis and comparison with 15N cross polarization/magic angle spinning nuclear magnetic resonance spectroscopy." Organic Geochemistry **36**(11): 1490-1497.

Abe, T. and A. Watanabe (2004). "X-ray photoelectron spectroscopy of nitrogen functional groups in soil humic acids." Soil Science **169**(1): 35-43.

Berman, T. and D. A. Bronk (2003). "Dissolved organic nitrogen: A dynamic participant in aquatic ecosystems." Aquatic Microbial Ecology **31**(3): 279-305.

Bu, L., et al. (2010). "Characterization of dissolved organic matter during landfill leachate treatment by sequencing batch reactor, aeration corrosive cell-Fenton, and granular activated carbon in series." Journal of Hazardous Materials **179**(1-3): 1096-1105.

Carlsson, P., et al. (1993). "Nitrogen bound to humic matter of terrestrial origin - a nitrogen pool for coastal phytoplankton?" Marine Ecology Progress Series **97**(2): 105-116.

Chan, C. C. P., et al. (2012). "Fabrication of amine-functionalized magnetite nanoparticles for water treatment processes." Journal of Nanoparticle Research **14**(4).

Chen, H. L., et al. (2010). "Characterization of dissolved organic matter derived from rice straw at different stages of decay." Journal of Soils and Sediments **10**(5): 915-922.

Eriksson, J., et al. (2004). "Binding of 2,4,6-trinitrotoluene, aniline, and nitrobenzene to dissolved and particulate soil organic matter." Environmental Science and Technology **38**(11): 3074-3080.

Fortner, J. D., et al. (2007). "Reaction of water-stable C60 aggregates with ozone." Environmental Science and Technology **41**(21): 7497-7502.

He, X. S., et al. (2011). "Physicochemical and spectroscopic characteristics of dissolved organic matter extracted from municipal solid waste (MSW) and their influence on the landfill biological stability." Bioresource Technology **102**(3): 2322-2327.

Huo, S., et al. (2008). "Characteristics of dissolved organic matter (DOM) in leachate with different landfill ages." Journal of Environmental Sciences **20**(4): 492-498.

Hwang, Y. S. and Q. Li (2010). "Characterizing photochemical transformation of aqueous nC60 under environmentally relevant conditions." Environmental Science and Technology **44**(8): 3008-3013.

Kaiser, E., et al. (2003). "Solid-state and multidimensional solution-state NMR of solid phase extracted and ultrafiltered riverine dissolved organic matter." Environmental Science and Technology **37**(13): 2929-2935.

Landry, C. and L. Tremblay (2012). "Compositional differences between size classes of dissolved organic matter from freshwater and seawater revealed by an HPLC-FTIR system." Environmental Science and Technology **46**(3): 1700-1707.

Liao, B. Q., et al. (2011). "Effects of temperature and dissolved oxygen on sludge properties and their role in bioflocculation and settling." Water Research **45**(2): 509-520.

Maie, N., et al. (2006). "Chemical characteristics of dissolved organic nitrogen in an oligotrophic subtropical coastal ecosystem." Geochimica et Cosmochimica Acta **70**(17): 4491-4506.

Matamoros, V. and V. Salvadó (2012). "Evaluation of the seasonal performance of a water reclamation pond-constructed wetland system for removing emerging contaminants." Chemosphere **86**(2): 111-117.

Minor, E. and B. Stephens (2008). "Dissolved organic matter characteristics within the Lake Superior watershed." Organic Geochemistry **39**(11): 1489-1501.

Pérez, M. A. P., et al. (2011). "Dissolved organic matter dynamic in the Amazon basin: Sorption by mineral surfaces." Chemical Geology **286**(3-4): 158-168.

Pernet-coudrier, B., et al. (2008). "Dissolved organic matter from treated effluent of a major wastewater treatment plant: Characterization and influence on copper toxicity." Chemosphere **73**(4): 593-599.

Provenzano, M. R., et al. (2010). "Dissolved organic matter extracted with water and a saline solution from different soil profiles." Soil Science **175**(6): 255-262.

Sansotera, M., et al. (2013). "Decomposition of perfluorooctanoic acid photocatalyzed by titanium dioxide: Chemical modification of the catalyst surface induced by fluoride ions." Applied Catalysis B: Environmental **148-149**: 29-35.

Seo, D. J., et al. (2007). "Characterization of dissolved organic matter in leachate discharged from final disposal sites which contained municipal solid waste incineration residues." Journal of Hazardous Materials **148**(3): 679-692.

Song, J., et al. (2012). "Chemical and isotopic composition of humic-like substances (HULIS) in ambient aerosols in Guangzhou, South China." Aerosol Science and Technology **46**(5): 533-546.

Stephens, B. M. and E. C. Minor (2010). "DOM characteristics along the continuum from river to receiving basin: A comparison of freshwater and saline transects." Aquatic Sciences **72**(4): 403-417.

Templier, J., et al. (2012). "Is nitrogen functionality responsible for contrasted responses of riverine dissolved organic matter in pyrolysis?" Journal of Analytical and Applied Pyrolysis **97**: 62-72.

Wang, L., et al. (2008). "Surface modification of polystyrene with atomic oxygen radical anions-dissolved solution." Applied Surface Science **254**(13): 4191-4200.

Wang, X., et al. (2013). "Variations in abundance and size distribution of carbohydrates in the lower Mississippi River, Pearl River and Bay of St Louis." Estuarine, Coastal and Shelf Science **126**: 61-69.

Wu, P., et al. (2011). "Effect of dissolved organic matter from Guangzhou landfill leachate on sorption of phenanthrene by Montmorillonite." Journal of Colloid and Interface Science **361**(2): 618-627.

Xi, B. D., et al. (2012). "The composition and mercury complexation characteristics of dissolved organic matter in landfill leachates with different ages." Ecotoxicology and Environmental Safety **86**: 227-232.

Xue, S., et al. (2009). "Chlorine reactivity and transformation of effluent dissolved organic fractions during chlorination." Desalination **249**(1): 63-71.

Xue, S., et al. (2011). "Comparison of dissolved organic matter fractions in a secondary effluent and a natural water." Environmental Monitoring and Assessment **180**(1-4): 371-383.

Yamashita, Y. and E. Tanoue (2003). "Chemical characterization of protein-like fluorophores in DOM in relation to aromatic amino acids." Marine Chemistry **82**(3-4): 255-271.

Zhang, H., et al. (2009). "Characterization of isolated fractions of dissolved organic matter from sewage treatment plant and the related disinfection by-products formation potential." Journal of Hazardous Materials **164**(2-3): 1433-1438.

Zhang, Y., et al. (2013). "Chemical and spectroscopic characterization of dissolved humic substances in a mangrove-fringed estuary in the eastern coast of Hainan Island, China." Chinese Journal of Oceanology and Limnology **31**(2): 454-463.

Zhang, Y. P., et al. (2013). "Distributions of dissolved monosaccharides and polysaccharides in the surface microlayer and surface water of the Jiaozhou Bay and its adjacent area." Continental Shelf Research **63**: 85-93.

Zhao, E., et al. (2008). "Surface modification of medical poly(vinyl chloride) with O-water." Journal of Applied Polymer Science **110**(1): 39-48.